Energy, Mines and Resources Canada | Énergie, Mines et Ressources Canada

CANMET

Canada Centre for Mineral and Energy Technology | Centre canadien de la technologie des minéraux et de l'énergie

ELECTRODES FOR SOLID ELECTROLYTES, - ELECTRODE MORPHOLOGY

J.D. Canaday and T.A. Wheat
Mineral Processing Laboratory

M.P. Haley and I.H. Joyce
Ontario Research Foundation

August 1987

This document is an unedited report prepared primarily for the use of the staff and contractors of the Canada Centre for Mineral and Energy Technology (CANMET)

Ce document est un rapport préparé principalement pour l'usage du personnel et des contractuels du Centre canadien de la technologie des minéraux et de l'énergie (CANMET)

Project: 3.0.2.9.0.1
Advanced Ceramic Materials

72 pp

MINERAL SCIENCES LABORATORIES
DIVISION REPORT MSL 87-106 (IR)

MICROMEDIA

ELECTRODES FOR SOLID ELECTROLYTES, - ELECTRODE MORPHOLOGY

by

J.D. Canaday and T.A. Wheat

Ceramic Section, Mineral Sciences Laboratory, CANMET

Department of Energy, Mines and Resources Canada

555 Booth Street, Ottawa, Ontario Canada, K1A 0G1

M.P. Haley* and I.H. Joyce

ABSTRACT

Using the techniques of image analysis, profilometry, gas permeability, mercury porosimetry, and gas adsorption, the morphological properties of porous electrode film (1-100 μm) materials are discussed.

The materials include platinum paste which is utilized as electrodes for high temperature, oxygen-ion-conducting ZrO_2 electrolytes and for low temperature hydronium - conducting Nasicon electrolytes. Also considered are plasma sprayed nickel and perovskite materials. In order to assess the possible correlation of morphological parameters, the measurements of silver membranes are presented. It is shown that each of the five methods can be used to make quantitative evaluations of thin-film electrodes. The parameters measured include particle diameter, pore diameter, porosity, three-phase line, thickness, surface texture, gas-flow/pressure, pore area, and surface area. These properties are related to the effects of activation polarization and concentration polarization which reduce the performance of electrochemical cells.

Keywords: electrode morphology, morphology, electrodes, solid electrolytes, electrochemical cell, hydronium electrolytes.

---

* Present address: Westroc Industries Limited, 2424 Lakeshore Road W., Mississauag, Ontario, L5J 1K4

ÉLECTRODES POUR LES ÉLECTROLYTES SOLIDES - MORPHOLOGIE DES ÉLECTRODES

par

J.D. Canaday et T.A. Wheat
Section des céramiques, Laboratoires des sciences minérales, CANMET
Énergie, Mines et Ressources Canada
555, rue Booth, Ottawa (Ontario) Canada, K1A 0G1
M.P. Haley* et I.H. Joyce

RÉSUMÉ

Dans le présent rapport, on traite des propriétés morphologiques de matériaux de pellicules (1-100 µm) d'électrodes poreuses en utilisant les techniques d'analyse par imagerie, de profilométrie, de perméabilité au gaz, de porosimétrie du mercure et d'adsorption du gaz.

Parmi ces matériaux, on compte la pâte de platine qui est utilisée comme électrodes pour des électrolytes de ZrO_2 conducteurs d'ion-oxygène à haute température et pour des électrolytes de Nasicon conducteurs d'hydronium à basse température. On étudie également le nickel et la pérovskite recouverts par pulvérisation de plasma. Afin d'évaluer la corrélation possible entre les paramètres morphologiques, on présente les mesures des membranes d'argent. On démontre que chacune des cinq méthodes peut être utilisée pour évaluer quantitativement les électrodes à pellicule mince. Les paramètres mesurés comprennent le diamètre des particules, le diamètre des pores, la porosité, la ligne de phase triple, l'épaisseur, la texture de la surface, la pression/débit du gaz, la surface poreuse et la surperficie. Ces propriétés sont reliées aux effets de la polarisation d'activation et de la polarisation de concentration qui réduisent la performance des piles électrochimiques.

Mots-clés : morphologie des électrodes, morphologie, électrodes, électrolytes solides, pile électrochimique, électrolytes d'hydronium.

---

*Adresse actuelle : Westroc Industries Limited, 2424, chemin Lakeshore ouest, Mississauga (Ontario) L5J 1K4.

1. INTRODUCTION

The morphology of the electrodes used in certain types of electrochemical cells has been known [1-9] to affect the performance of these devices. Of particular interest here is the three-phase cell consisting of a solid (ceramic) electrolyte (in which mobile ionic species migrate or diffuse), porous metal electrodes and reactant gas species. This structure may be compared with two-phase electrochemical cells containing a liquid or solid electrolyte and non-porous metal electrodes.

A number of three-phase cells has been under intensive study. The cell with doped ZrO_2 [1-9] as the electrolyte is an anionic conductor, having O^{2-} ions as the mobile species. The operating temperature of this cell is 800-1000°C. A cationically conducting cell based on the $SrCeO_3$ electrolyte [10-13] also operates in this temperature range and has protons as its mobile species.

Two protonic conductors which operate at 100-300°C have also been developed. The β/β -Al_2O_3 [14-16] and Nasicon [17-18] formulations show promise as precursor electrolytes for fuel cells, electrolyzers and sensors. In order for these materials to be used in hydrogen cells, it is necessary for the mobile cationic species to be exchanged for hydronium, H_3O^+, ions. A method for ion-exchanging the precursor material in powder form and then bonding the exchanged powder with an inorganic substance has been developed [19].

A number of electrochemical devices have been reported which utilize the hydronium electrolyte. Reviews of cell components and device applications are available [20-22]. The use of the Nasicon electrolyte in a hydrogen sensor and a hydrogen pump [23] has been shown. As a sensor, the Nernstian behaviour was approximated, and when operated as a pump, a current density of 10 mA/cm^2 was obtained at 30 V. Additional studies of hydrogen electrolysis have been made [24] in which a current of 200 mA passed and where the electrolysis proceeded with an efficiency of 100%. When operated as a fuel cell [25], an open circuit voltage of 0.8 V and a maximum current density of 0.3 mA were obtained. The water-electrolysis and fuel-cell characteristics of the H_3O^+ β/β"-Al_2O_3 cell have also been described [26].

The interrelationships between electrode morphology and polarization mechanism have been discussed and summarized for the Pt/ZrO_2 system [7]. In

this study, a number of very different morphologies were considered; they included porous paste, non-porous foil, sputtered electrodes and point electrodes. For the temperature range, oxygen pressure, and current density associated with each of these morphologies, the rate-limiting or polarization mechanisms were discussed.

Subsequent investigations of the ZrO_2 electrolyte have been made with platinum paste as the most common electrode material. At high oxygen pressures, the current over-potential curves were found to obey the Butler-Volmer equation which implied a charge transfer (or activation) polarization [27]. Also in this study, it was found that at low oxygen pressure, a limiting-current behaviour resulted which was characteristic of cathodic concentration polarization. Similar conclusions were reached [28] regarding the effect of oxygen pressure in an analysis which contained measurements of the two-phase contact area and the length of the three-phase line. In an additional study, [29], a model was proposed in which a fraction of the oxygen molecules arriving at the three-phase line is ionized directly and enters the electrolyte and a second part diffuses as oxygen atoms along the two-phase interface before being ionized. Recently, some of the previous results, [28], have been reinterpreted in view of newer models and experiments [8,9]. It was claimed that charge-transfer kinetics cannot be the rate-determining step of the electrode reaction even at high oxygen pressure. Rather, the reaction proceedes by the surface diffusion of adsorbed oxygen atoms on platinum and by the dissociative adsorption of oxygen gas molecules near the three-phase line.

In this investigation, the need for thin film characterization has been driven by the demand in the electrochemical sciences to better understand the dependence of physical morphology on the operational behaviour of porous electrodes. The efficiency of these devices can be limited by the physical structure of the electrode. The development of suitable characterization techniques will obviously lead to better control of the morphology of formed electrodes, resulting in a means to evaluate alternative electrode compositions. This has the potential effect of increasing device efficiency while improving overall cell viability (i.e., material cost, assembly methods, lifetime, and reliability).

The objective of this collaborative program, therefore, has been to identify, develop, refine, and implement characterization techniques which

will quantitatively determine the physical structure of electrode film materials in a reliable and reproducible manner. Five techniques have been utilized to measure the properties of electrode materials; they are image analysis, profilometry, gas permeability, mercury porosimetry, and gas adsorption.

2. MORPHOLOGICAL PARAMETERS AND ELECTROCHEMICAL PROCESSES

The electrode morphological parameters considered here are shown schematically in Fig. 1(a). An obviously important feature of an electrode is its thickness. The distinction between thin films and thick films, when seen in the context of solid-state devices is somewhat arbitrary. The former may be considered to have a thickness of less than 1 μm. Electrodes in this category are often deposited by the sputtering process. Thick-film electrodes, with thicknesses of 1-100 μm, are deposited as pastes or by the plasma spray method. With porous electrodes, the pore diameter, particle diameter, percent porosity, and surface area can also be measured. At the interface between an electrode particle and the electrolyte substrate is the two-phase contact area which is shown in Fig. 1(b). The perimeter of this region is known as the three-phase line where the electrode, electrolyte, and reactant gas phases are in mutual contact.

In electrochemical terms [30], the three-phase system can be considered as two distinctive catalytic regions. One region is the gas-platinum interface where the reactant gas species is adsorbed on the surface of the electrode platinum particles. Here, chemical reactions such as dissociation, $H_2 \rightleftharpoons 2H$ or $O_2 \rightleftharpoons 2O$, occur. In this two-phase region, platinum is acting as a heterogeneous catalyst. The second region is the interface between the platinum and the electrolyte where the electrode particle is acting as an electrocatalyst. Here, ions within the electrolyte, when reaching the interface, participate in charge transfer or reduction-oxidation (redox) reactions. Presumably, along the three-phase perimeter of the platinum particles, both types of catalytic processes occur. A model of these processes has been developed [29] for the reduction of oxygen in the Pt/ZrO_2 system. From a visualization of these concepts, it is evident that lower electrical currents will occur when the electrode is a continuous (non-porous) foil rather than a porous structure. This result has been demonstrated [31] for the Pt/ZrO_2 cell. In theory, at least, it

appears possible to develop an optimization of particle size, porosity, two-phase contact area, and three-phase line which would lead to a maximum electrical current density.

For a two-phase, metal-electrode/liquid electrolyte system, the general equation [32] for the molar flux of a species in one dimension is:

$$J = Cv - D\frac{dC}{dx} - \frac{ZF}{RT} DC \frac{dV}{dx} \qquad (1)$$

where the three terms represent convectional, diffusional, and migrational proceses respectively. The concentration of the species is given by C, the linear velocity is v, and the diffusion coefficient is D. The negative signs of the diffusion and migration terms indicate that material and charge is being transported away from the electrode. Faraday,s constant, 96,485 coulombs/mole, the electric charge, gas constant, and absolute temperature are given by F, Z, R, and T respectively.

The three-phase system consisting of an ideal reactant gas at a partial pressure, P, a porous metal electrode, and a solid electrolyte can be modelled analogously to the terms of equation (1) by similar relations, for convection, diffusion, and migration. The convective term for molecular gas flow outside the cell is:

$$J_c = \frac{P}{RT} \frac{f}{A} \qquad (2)$$

The linear velocity is v = f/A where f is the volumetric flow rate, and A is the cross-sectional area of the electrode. Two diffusive processes may be considered for the electrode. Diffusion of the gas phase is described [5,20,33] by the relation:

$$J_g = \frac{D_g}{RT} \frac{dP}{dx} p \qquad (3)$$

where D_g is the gas diffusion constant, dP/dx, replacing the concentration gradient, is the partial pressure gradient which is measured from the electrode's outer surface to the electrode-electrolyte interface, and p is

porosity of the electrode. For self-diffusion of like molecules, the coefficient is given [33] by:

$$D_{1,1} = \frac{\bar{v}\lambda_{1,1}}{3} \tag{4}$$

where $\bar{v}$ is the average molecular velocity assuming a Maxwell-Boltzmann distribution. The term $\lambda_{1,1}$ is the mean free path between collisions of like molecules. For the interdiffusion of two different gas species, the coefficient, $D_{1,2}$ is used [33]. If the mean free path between collisions is larger than the pore radius, r, then Knudsen diffusion results in which the diffusion coefficient is given by:

$$D_K = \frac{2}{3} \bar{v} r, \; r < \lambda \tag{5}$$

An second diffusional term is present when electrochemical species diffuse on the surface of the electrode or the electrolyte. This process has been considered [29] for diffusion along the three-phase line, L, according to the relation:

$$J_s = D_s L \frac{dC}{dx} \tag{6}$$

where D_S is the surface diffusion coefficient. The electric current density for equations (2), (3), and (6) is obtained from the relation:

$$J = n_e F J_m$$

where n_e is the number of electric charges transferred during the electrochemical reaction, F is Faraday's constant, 96,485 coulombs/mole, and J_m is the molar flux density. The migrational term of the electrolyte can also be written as Ohm's law:

$$J = q \mu n E \tag{7}$$

in which q is the electric charge, μ is the mobility, n is the number density of the carriers, and E is the electric field or the voltage gradient, dV/dx.

In addition to convection, diffusion and migration, a charge-transfer mechanism occurs which is of the form $O + ne \rightleftharpoons R$. Here, O represents the oxidized species, ne is the number of electrons transferred, and R is the reduced species. This mechanism is modelled [27,28] by the Butler-Volmer equation [30]:

$$J_e = J_{o,e} \left[\exp \left(\frac{\alpha_a F \eta_a}{RT} \right) - \exp \left(\frac{-\alpha_c F \eta_c}{RT} \right) \right] \tag{8}$$

and occurs at the three-phase line and/or at the two-phase contact area. In this relation, $J_{o,e}$ is the exchange current density, α_a and α_c are the anodic and cathodic transfer coefficients; η_a and η_c are the anodic and cathodic overpotentials.

3. POLARIZATION MECHANISMS

The operating voltage of an electrochemical cell, V_{cell}, is altered from its equilibrium or open-circuit value, V_{eq}, by polarization mechanisms, V_p, according [34] to the equation:

$$V_{cell} = V_{eq} \pm V_p \tag{9}$$

The positive sign applies to externally driven cells, as in the case of electrolysis, and the negative sign is used for internally driven devices such as fuel cells.

Polarization mechanisms are a result of electrochemical process limitations; that is, slow processes (or low current densities) are manifested as large polarization voltages. Three mechanisms have been generally identified to occur in electrochemical cells. Concentration polarization results from a limitation of diffusing species either within the porous region of the electrode or at the interface. The term "ohmic

polarization" has been applied to the migrational process of the electrolyte even though the polarization phenomena are more appropriately associated with the electrodes. The limitation due to the charge transfer process is known as activation polarization. The functional relations for these mechanisms are well known [34] and they combine to give a total cell polarization:

$$V_p = V_{conc} + IR + V_{act} \tag{10}$$

where the term V_{conc} represents concentration polarization, IR is the ohmic loss of the electrolyte, and V_{act} is referred to as the activation polarization.

Table 1 summarizes the various processes and polarization mechanisms as well as the controlling morphological parameters and measurement techniques.

4. PHYSICAL CHARACTERIZATION TECHNIQUES

The evaluation of physical morphology for thin film materials places certain demands on the characterization techniques employed. In most cases, conventional methods which were developed for evaluating bulk materials have certain limitations on sample size (volume). The approach of this study has been to modify and extend standard techniques, such that relevant physical data on thin film materials could be obtained. In many cases, the selected techniques were employed to examine the same morphological parameters from a different perspective. In these situations, attempts to correlate the results should provide some degree of validity for employing these methods.

4.1 Image Analysis

Image analysis is a quantitative technique for evaluating the size and/or shape of features in an image. The process involves inputting a video image, which may be from a camera (scanner), SEM, or direct video link, to a computer which can generally store the image. Once the image is stored digitally by the computer, its composition can be broken down into what is known as a grey-level map which assigns a distinct (generally 0-255) grey level to each pixel element (a standard video monitor would have approx. 250,000 pixels). The image can then

Table 1. - Electrochemical Process, Polarization Mechanisms, Morphological Parameters, and Measurement Techniques

Process	Polarization Mechanism	Controlling Morphological Parameter	Measurement Technique
Convection	Concentration - if gas flow rate inadequate	None - gas flow is external to cell	Not applicable
Gas Diffusion of molecular species in porous region of electrode Self-diffusion, $r > \lambda$ Inter-diffusion, $r > \lambda$ Knudsen diffusion, $r < \lambda$	Concentration	Electrode thickness Porosity Pore size Tortuosity	Image analysis Profilometry Gas permeaability Mercury porosimetry Gas adsorption
Surface diffusion of species on electrode	Concentration	Particle size	Image analysis
Surface diffusion of species on electrolyte	Concentration	Two-phase contact area	Image analysis
Surface diffusion of species along three phase line	Concentration	Three-phase line	Image analysis
Charge transfer	Activation	Two-phase contact area Three-phase line	Image analysis Image analysis
Catalytic activity Heterogeneous catalysis	Not defined. Capacitive effects appear as imaginary impedance components	Particle size Surface area	Image analysis Mercury porosimetry Gas adsorption
Electrocatalysis Migration of ionic species through electrolyte	Ohmic	Two-phase contact area Electrolyte thickness	Image analysis Profilometry for thin-film electrolyte

be "thresholded" to group certain grey-levels together, thereby discriminating between different features of interest. Most modern digital image analyzers currently available also offer various degrees of image processing which can be employed to enhance the image and highlight certain features which are difficult to distinguish otherwise. The image processing capabilities can include erosion/dilation for separating touching features, logical functions for comparing images or adjusting for shading, small feature enhancement to emphasize minute details, filtering to smoothen "rough" edges, and grey-level equalization to improve the contrast of all features.

Once the image has been processed for the features of interest, it is possible to perform an analysis which will give quantitative information such as the percent area (or porosity), length, width, aspect ratio, orientation, or perimeter. Other perimeters or combination of parameters (e.g., shape descriptors, fractals, etc.) can also be obtained by modifying the analysis program.

The Ontario Research Foundation currently maintains a LeMont Scientific [36] OASYS image analyzing computer which is equipped with a Newvicon tube scaner (camera), 4MB memory (15 image storage), and high resolution (0.001") digitizing tablet (digipad). Analysis software which has been employed in this project to study pore and/or particle dimensions includes a lineal program (chord-length), line scan program, and diameter program (minimum crossing diameter). The operation and application of each of these programs, are discussed in the following sections.

4.1.1 Lineal Analysis

Lineal analysis, also known as cross section chord length or stereological analysis, provides a quantitative evaluation of feature width at pre-described scan lines along either the horizontal or vertical scan direction. Basically, after the features of interest are thresholded, the image is scanned and this technique can measure the chord lengths of recording the number of "on" and "off" points (pixels). By setting the number of scan lines, it is possible to control the number of features or rather the number of chords analyzed.

Data generated from such an analysis include chord length distribution, average chord length, volume fraction, number of features, edge-to-edge spacing, center to center spacing and surface-to-volume ratio. When applied to the pores and particles of the cross-sectioned films studied in this program, information on the pore/particle diameters as well as the void/solid volume (% porosity) can be obtained.

4.1.2 Line Scan Analysis

The line scan analysis program was originally developed for the simultaneous measurement of features containing two or more intensity levels. To do this, the image analyzer keeps track of every line scan (512 horizontal lines) and determines the area and perimeter points of adjacent lines which are thresholded. By storing the perimeter points of all features it is possible to derive such parameters as Ferets diameter (maximum length), width (at right angles to length), and orientation (degrees 0°-360°) of maximum axis as well as perimeter length. Other parameters include percent area (percent porosity for pore analysis) and shape (width-to-length ratio). For the purpose of this program, area equivalent diameter (the diameter of a circle having the same area as the particle/pore) and area percent (porosity) were employed for characterizing film morphology. In most cases however, this analysis can only be applied to non-continuous features with many inclusions. For these situations, the lineal or diameter analysis may be more appropriate.

4.1.3 Diameter Analysis

The diameter analysis program involves determining the approximate centroid of detected features and then constructing a chord length or diameter length assessment through this point.

4.1.4 Sample Preparation

As stated earlier, the image generated for subsequent analysis can come from a variety of sources, however, it is imperative that the technique employed be selected to provide the maximum degree of contrast between the features of interest and the background. For

features which are small in size and have different chemical compositions, SEM examination (particularly backscattered electron (BSE images) will usually provide sufficient contrast. For materials of varying refractive index or coloration, optical microscopy can often be employed. Either of these approaches can be used directly (i.e., SEM/IA interface, optical microscope/camera) or indirectly through the use of photomicrographs which can be input to the image analyzer thorugh a camera/lens arrangement.

Some problems arise, however when examining pores or the nature of porous bodies. Since, in fact, there is nothing to measure or observe, distinguishing phase boundaries can be extremely difficult if not impossible. It therefore becomes necessary to impregnate the sample with a material that will permit feature identification. This mounting procedure has become standard practice in metallurgical studies and generally involves filling the voids with a liquid epoxy which sets in the pores.

When the porous features becomes sufficiently small, it is usually necessary to employ a special low-viscosity mounting medium coupled with vacuum or centrifuge impregnation [36] and/or pressure curing [37]. Set samples can then be cross-sectioned and polished to provide a two-dimensional picture of the porous nature of the sample. With elaborate computer software and controlled cross-sectional analysis, it is also possible to re-construct three-dimensional representations from a series of two-dimensional images.

In this study, porous films were vacuum impregnated and pressure cured with Spurr Low-Viscosity Embedding Media [38] and subsequently cross-sectioned and polished for examination under either the SEM or optical microscope. Quantitative measurements were performed on the two-dimensional images using the techniques described previously.

4.2 Profilometry

Analysis of surface texture has become an important engineering consideration especially when one is examining the interaction between two materials. The measurement of surface texture can be accomplished by a variety of analytical techniques utilizing optical, contact,

electrical, and fluid methods [39]. The most widely employed technique, however, is that using the stylus tracking instrument which is generally referred to as profilometry.

Profilometry offers the advantage of being a simple, proven, and relatively non-destructive means of evaluating differences between bulk materials. In this study, it was hoped that some correlations could be drawn to relate the surface texture of a porous film to its internal porosity or pore structure as measured by an alternative technique such as permeametry or surface area analysis. This relationship was expected to exist for films that were deposited by a random process, when the exposed surface closely approximates the morphology of underlying layers.

In quantifying physical surfaces by profilometry it is important to remember that a profilometry trace is a simple scan "snapshot" of the surface on a predetermined line and that the roughness of a surface cannot be adequately described by one parameter. This implies that the measurement of surface roughness is a statistical process in which a number of parameters must be computed. Parameters are therefore best reported as mean values with associated standard deviations for the area of the surface scanned (or number of traces performed).

The Ontario Research Foundation currently operates a Rank Taylor Hobson Talysurf 6 profilometer [40]. The unit is equipped with the Talydata 2000 computer for calculating over twenty-five surface texture parameters and information on bearing ratios and profile cross-sections. The Talysurf 6 is also capable of operating in a statistical acquisition mode with a variety of stylii (low magnification tip approx. 12 µm to high resolution tip approximately 1.5 µm diameter). To better understand the measurements given as part of this study, the following sections address some of the more important considerations in conducting and reporting profilometry analyses.

4.2.1 Profile Filtering

Any two dimensional surface can be considered to have three types of surface structure; microstructure, which can be referred to as texture or roughness and two macrostructure variables which are

termed waviness and form over which roughness is superimposed. To differentiate texture from waviness and form, it is necessary to damp out these secondary effects through the use of filtering.

There are three basic types of filtering commonly used in profilometry; mechanical, graphical, and electrical. The latter technique involves passing the stylus transducer output through a resistor-capicitor circuit. Since this approach has not been employed in the study, it will not be considered further.

Mechanical filtering involves the use of a support mechanism known as a skid. Basically the skid supports the stylus arm such that the stylus head is free to follow the movement of the skid over the form or waviness of the surface. Since the whole assembly is free to move along the peaks and valleys of the form, the stylus movement is dampened. The degree of dampening or filtering is affected by the skid to stylus distance as well as the nature of the surface. Since the skid and the stylus cannot touch the surface at the same point, there is a phase effect which is dependent upon the movement of the skid and stylus as well as the amplitude.

Graphical filtering involves correcting for any waviness or form by dividing the total scan length into a series of sampling lengths for which texture parameters are computed independently. By segmenting the profile into smaller sampling lengths and calculating the center line average (CLA) for each length, the trace can be replotted by joining all the mean lines to form a continuous CLA. This removes the waviness effect from the profile.

4.2.2 Surface Texture Parameters

As mentioned before, the Talysurf 6 system is capable of assessing over 25 standard surface texture parameters which all define some unique properties of the surface. Computed values are generally broken into three classifications; 1) amplitude parameters which are solely dependent upon the vertical displacement of the profile, 2) spacing parameters which are measures of irregularity spacings along the surface, irrespective of the amplitude of the irregularities, and 3) hybrid parameters, which relate to both the amplitude and spacing of surface features. A listing of the standard

surface texture parameters, together with their meaning and method of calculation, is provided elsewhere [41].

4.3 Gas Permeability

The application of gas permeability (or permeametry), or fluid flow studies, has long been employed to evaluate relative differences between porous materials. Since permeability measurements are extremely sensitive to small changes in pore geometry, this technique can be applied to the characterization of pore structure in permeable materials. When gases are employed (as opposed to liquids), however, complications can arise due to the laws governing gas flow which vary with the pressures employed and the pore dimensions.

Fluid flow in single capillaries can be classified into four regimes; turbulent, viscous or laminar (Poiseuille), slip flow, and molecular streaming (Knudsen flow). Turbulent flow occurs at high pressures and results in energy losses which produce a non-linear relation between mass flow and pressure. During laminar flow, the mass flow and pressure are directly proportional (linear). As the pressure or capillary size decreases further, there is an increase in mass flow due to slippage at the boundary, and when the mean free path of the gas is approximately ten times the diameter of the capillary, molecular diffusion prevails. In order, therefore, to draw conclusions regarding pore structure without using complex models, it becomes necessary to operate in the region where simple linear equations relate mass flow, pressure, and pore dimensions.

The relation which governs permeability in this region is given by the Poiseuille equation:

$$Q = \frac{\pi r^4}{8\eta} \cdot \frac{\Delta P}{L} \qquad (11)$$

when Q is the volume of fluid flowing per unit time, r is the radius of the pore, η is the fluid viscosity, Δp is the pressure differential across the material, and L is the length of the sample (pore).

If a porous medium is treated as a bundle of uniform parallel capillaries, N_o, of radius r, then:

$$Q = \frac{\alpha A\, N_o r^2}{8\eta} \cdot \frac{\Delta P}{L} \qquad (12)$$

Here A refers to the cross-sectional area of a pore ($A = \pi r^2$) and α is the fractional void area (i.e., percentage of open area across the sample surface). By plotting Q *vs* ΔP, one should therefore obtain a linear relationship, assuming laminar flow. More complete descriptions of these and other theoretical equations including slip flow and molecular diffusion models may be found elsewhere [42].

For this program, permeametry was seen to be a plausible method for evaluating the reproducibility of preparing porous gas electrode materials of uniform bulk morphology. This technique, however, was somewhat limited in that it was necessary to conduct the analyses on unsupported materials since the presence of any support would seriously influence the observed permeability behaviour by either superimposing the flow characteristics of the support on that of the film or by altering the pore structure of the film as it was deposited on the support. Calibration measurements were made using Millipore [43] and Nuclepore membranes [44].

4.4 Mercury Porosimetry

The application of mercury porosimetry for evaluating the pore size distribution and total porosity of bulk materials has become a routine analytical technique. The principle is based upon the capillary rise phenomenon whereby an excess pressure is required to cause a non-wetting liquid to climb up a narrow capillary. For cylindrical pores, the pressure P, required to drive mercury into a pore of radius r, is related to the contact angle, θ, between the liquid and solid, and the surface tension of the liquid, γ, by the Washburn equation [45]:

$$P = \frac{2\gamma}{r} \cos\theta \qquad (13)$$

To obtain a complete pore size distribution, the cumulative volume of intruded liquid is measured with increasing pressure which can be related to pore size by equation (13). This corresponds to what is known as an intrusion curve. It is also possible to monitor the volume of liquid expelled by a porous material when the pressure is decreased. The result is termed an extrusion curve. The intrusion and extrusion curves do not necessarily coincide and some type of hysteresis generally exists. Factors such as changing contact angle [46], pore shape [47], and pore potential [48] are all plausible explanations that have been put forward to account for this effect.

Since mercury exhibits a greater contact angle with more materials than any other conveniently usable liquid, it is almost universally employed for the evaluation of pore sizes by the pressure penetration technique. It is also a very suitable liquid for monitoring volume intrusion/extrusion by electrical means since it is a conductive material.

In this work, a Micromeritics Autopore 9200 porosimeter [49] was used. This unit is capable of operating up to pressures of 60,000 psia, which for mercury on a solid with a contact angle of 130°, corresponds to a smallest intruded pore dimension of 0.003 μm or 30A. In conducting an analysis, a weighed portion of sample is placed inside a penetrometer vessel. The penetrometer is sealed at one end with the conductive cap and subjected to a vacuum to remove residual air and/or adsorbed species from the porous sample. Without performing this evacuation, air trapped in the pores will be compressed at higher pressures thereby leading to erroneous results.

Following evacuation, the penetrometer is filled with mercury such that the small capillary is completely full. The penetrometer is then placed in a hydraulic oil chamber such that an increase in oil pressure will drive the mercury down the capillary and into the sample. The advantage of using mercury is apparent here since the volume of mercury pushed into the sample can be monitored by measuring the change in capacitance between the moving column of mercury and the external conducting sheath. By knowing the exact dimensions of the capillary, it is therefore possible to calibrate the penetrometers such that precise volume measurements can be made.

Commercial penetrometers are available in a variety of sample chamber sizes and capillary volumes ranging from 3 to 15 cc, and 0.38 to 1.8 cc, respectively. Unfortunately, these penetrometers have been designed to measure the porosity of bulk materials (i.e., grains of sample) as well as samples with significant porosity. Problems are therefore encountered when one attempts to measure either non-porous materials or samples with small volumes, such as films, since there is not enought void volume to obtain a measurable intrusion using standard diameter penetrometers (smallest = 1.5 mm).

For example, if one considers a 25 mm diameter film with a thickness of 100 μm and a porosity of 10%, the total available volume for intrusion is 0.049 cm^3 or approximately 13% of the total capillary volume for the most sensitive commercial penetrometer. Further, if the thickness or porosity decreases then the percent change in mercury moving down the standard capillary becomes practically insignificant.

There are two ways to solve this dilemma. Firstly, one could increase the total volume of sample by adding more films. This approach, however, results in a blending of data for the entire set of films which will not provide any information on the variability of individual films. The second method involves designing a high pressure penetrometer with an even narrower bore than commercially available. This latter approach was taken as part of this program.

In conjunction with the manufacturer (Micromeritics), ORF was able to obtain a set of narrow-bore penetrometers with a capillary dimension of approximately 0.5 mm. This corresponds to an almost tenfold increase in sensitivity which, if used for the example cited above, would result in an overflow situation where all of the mercury in the capillary would be intruded into the sample.

Unfortunately, the development of these penetrometers has led to new problems in performing the intrusion analyses. Since the penetrometer now has an increased sensitivity, effects which were insignificant with regular penetrometers are now major problems. These effects arise from incomplete filling of the penetrometer resulting in measurable "intrusion" as the pressure increases from 1 to 30 psia (175 μm - 6 μm) and high pressure compression which result in another

measurable intrusion between approximately 2500-60,000 psia (0.07 - 0.03 μm). This has the total effect of severely limiting the range of reliable measurements from about 30 psi to 1500 psi (6 - 0.12 μm). Beyond this range, the observed intrusion will be compounded and absolute measurements should be suspect, althcugh the approach could still be employed in a relative manner to examine significant differences in micro-pore structure.

Previous research conducted at Atomic Energy Canada Limited in Chalk River, Ontario [50] led to the development of a novel approach for monitoring the filling of pores in micro-thin films. This technique involved the measurement of electrical impedance changes in a film as mercury is forced into the pores of the sample. Since the means of accurately measuring the mercury volume intruded has been the limiting factor for conventional porosimetry, this electrical approach provided the measurement in an elegant and extremely sensitive manner.

Preliminary investigations of this technique at ORF involved using a HP 4192A LF Impedance Analyzer coupled to platinum paste films screen-printed on penetrometer caps. In the first series of tests, the Micromeritics Auto Pore was employed to generate mercury intrusion into the sample, however, problems were encountered in impedance reading stability (both resistive and capacitative components). This was thought to be caused by parallel circuit problems which resulted from using the instrument ground as a conducting medium.

Further attempts were made to employ this technique by using an older Aminco 60,000 mercury porosimeter. This instrument offered the advantage of being able to electrically isolate the impedance measurement circuit. Unfortunately, the technique was still found to be quite unstable, possibly due to thermal effects in the hydraulic oil/mercury or the polarization of mercury.

Although the original work in this area examined the pore structure of insulating films (e.g., oxides), it was thought that the technique could be applied to conductive films as well, assuming that the conductivity of mercury was much greater than the conductivity of the film. Unfortunately, due to the stability problems described above, the technique could not be proven conclusively and further study in this area has been suspended.

4.5 Gas Adsorption

When a solid is exposed to a gas, the gas molecules will impinge upon its surface, and depending upon the nature of the solid and gas as well as the pressure and temperature, these molecules will have a finite residence time on the surface. This phenomenon is known as adsorption which differs from absorption in which the gas molecules are actually taken into the body of the solid.

By monitoring the volume of gas adsorbed on a surface against the adsorption pressure (relative to the saturation pressure of the gas), it is possible to construct an adsorption isotherm. Measuring the volulme of gas adsorbed can be done by a number of conventional methods including: 1) the mass change of the sample can be monitored (gravimetric determination), 2) the pressure change of a closed system can be recorded (volumetric determination), or, 3) the amount of gas removed from a flowing stream can be detected (thermoelectric mass flow determination). In each case the measurement can provide one point on the adsorption isotherm which can be employed to reveal information regarding surface area, pore size distribution, and total pore volume.

The determination of surface area from adsorption isotherms has been examined extensively elsewhere [51], and a number of theoretical models currently exist for its evaluation. The most widely employed technique, however, is that known as multilayer adsorption which was originally proposed by Brunauer, Emmett, and Teller [52] and is commonly referred to as the BET theory. Using this approach, it is possible to employ the linear portion of a Type II isotherm (0.05 - 0.35 P/Po, where Po is the saturation pressure) to obtain an estimate of the volume of gas needed to produce a monolayer coverage over the entire surface area of the sample.

By measuring the total volume of gas adsorbed by the sample at a point slightly less than saturation pressure, the pore volume of a material can also be computed. In addition, by employing a modification of the Kelvin equation which relates relative pressure to the surface tension, contact angle, temperature and pore radius of gases as they condense in a cylindrical capillary, it is possible to compute a pore size distribution. (Incidentially, the Kelvin equation was the basis for Washburn's work on the theoretical model for mercury

porosimetry).

The selection of adsorbing gas (adsorbate) will generally depend upon the nature of the solid (adsorbent) and the conditions one wishes to employ. A variety of gases have been employed over the years with mixed results. These gases include water vapour, n-butane, freon, toluene, benzene, ethyl iodide, n-hexane, xenon, and argon. The gases generally employed, however, are nitrogen and krypton.

Nitrogen adsorption has become the accepted standard for the measurement of surface with an absolute surface area greater than 5 m^2. This is due to the accuracy by which the cross-sectional area of the nitrogen molecule is known (16.2 A) as well as the availability of liquid nitrogen which is used as a means of reducing the sample temperature to -196°C. The cooling permits pore condensation which can be detected and plotted as an adsorption isotherm.

For materials with absolute surface areas less than 5 m^2, krypton is usually employed since it has a saturation pressure of about 2.3 mm Hg at -196°C as compared to 729 mm Hg for nitrogen at the same temperature. This lower pressure minimizes the "dead space correction" in which the volume of the sample chamber can greatly influence the ability to obtain precise pressure differentials. One difficulty with using krypton, however, is that at liquid nitrogen temperatures, krypton solidifies (triple point = -157°C). The solidification therefore prohibits its application as an adsorbate for pore volume or size distribution measurements.

Micromeritics Orr Pore-Volume Surface-Area Analyzer Model 2100 was utilized for conducting standard gas adsorption studies. The unit is equipped with both krypton and nitrogen as adsorbates and employs a volumetric technique for measuring the volume of gas adsorbed on solid samples. The measurements are obtained by monitoring the pressure changes in an accurately known dead space, which is caused by the absorption of gaseous molecules on the cooled sample surface. Pressure changes down to 10^{-4} Torr can be monitored by a capacitance transducer type barometer. Measurement of samples with an absolute surface area of down to 0.1 m^2 can thus be obtained.

A limitation encountered with the commercial equipment employed at ORF was the design of the standard glass adsorption cells which were

constructed primarily for the analysis of powders or solids having a maximum dimension of less than 5 mm. This arrangement did not permit the measurement of larger films (i.e., 1" diameter); therefore a series of special sample cells was constructed. These cells contained a ground glass conical joint seal with an internal dimension of approximately 30 mm. This custom-designed cell was capable of storing a multitude of thin films (up to approximately 10 cm in stacked height) with a diameter of approximately 25 mm). This arrangement allows for the absolute surface area to be increased into a measurable range for krypton analysis.

It should be pointed out that the surface area of individual films (assuming an absolute area of less than 0.1 m^2) could not be measured. This limitation could be overcome with the design of a UHV system containing a small dead volume, more accurate pressure transducers, and a possible change of the adsorbate gas to xenon. The construction of this system was beyond the scope of this program; however, it should be seriously considered for future studies since it does provide a rapid and non-destructive technique for evaluating the physical morphology of thin films.

5. EXPERIMENTAL RESULTS ON THIN FILM MATERIALS

To study the feasibility of employing these characterization techniques a number of films with various morphologies and compositions (including films prepared in different manners) were investigated. The first materials studied were platinum paste films since they are currently being used as electrodes in the electrochemical cell development program at CANMET. Plasma spraying as a deposition method was examined by evaluating porous nickel films prepared by this process. Some preliminary analyses were also conducted on perovskite coatings (films) produced by the plasma spray technique. Finally, in an effort to standardize and correlate the analyses procedures, a number of controlled morphology silver membrane filters were investigated.

5.1 Platinum Paste Films

To date, cell studies at CANMET have been conducted primarily with platinum as both the cathode and anode material, the majority of

which are platinum pastes or inks developed by Engelhard [53]. These materials are available in a wide variety of compositions and particle sizes. Special inks such as Englehard #6926 or A-4338 have been specifically developed for oxygen sensing applications when used as electrodes for zirconia electrolytes. These pastes have been designed primarily for brush applications but are certainly amenable to screen-printing. Screen-printing offers the advantages of controlled area application as well as uniformity in applied thickness and texture. Screen-printing also allows for the production of reproducible films with a defined morphological nature.

A limitation facing the development of electrode materials for use in the hydronium exchanged solid-state cell, is the sensitivity of the electrolyte to temperatures greater than approximately 150°C. This constraint is believed to limit the performance of the platinum pastes since they are designed primarily for high temperature applications and should be fired in excess of 800°C to realize their full conductivity and catalytic reaction activity.

On a macroscopic scale, the #6926 ink has a tendency to form isolated islands of film which severely affect the overall conductivity. Figure 2 shows a 60% 6926 paste (40% toluene) which has been screen-printed on α-alumina and then cured in air at 500°C and 800°C, respectively. Depending upon the film thickness, the degree of particle separation may become so great as to restrict all conductivity. This behaviour has also been observed when the 6926 paste was cured in hydrogen at a lower temperature (200°C).

SEM examination of the A-4338 pastes reveals an equally interesting change in film morphology of firing at various temperatures. Figures 3 and 4 show the A-4338 paste after screen printing on α-alumina and curing at 100°C and 800°C. Firing above 600°C appears to produce a highly irregular but porous film with good interconnectivity. This was further confirmed by two-point resistance measurements which showed a decrease in resistance from approximately 40 Ω/cm to 0.8 Ω/cm for the temperature curing range of 100°C to 800°C. Curing in hydrogen at 200°C also gives a film with good conductive properties and a relatively porous structure. The A-4338 ink is known to contain a finer grind of platinum particles (50%

approx. 2-4 μm) in comparison to the #6926 paste which has a mean size of ~12 μm. This would most likely contribute significantly to the overall performance of the ink as a fuel cell electrode, particularly for low temperature applications.

5.1.1 Image Analysis of Platinum Paste Films

From Figures 3 and 4 it can be seen that any pores which do exist within the platinum paste film are of the order of 1 μm in diameter. Due to the fine nature of these pores, regular epoxy mounting and polishing was unsuccessful in producing a cross-sectioned plane which had sufficient contrast between pores and particles. Viewed under the SEM, the polished samples appeared blurred and smeared such that no pore structure could be measured quantitatively.

In an effort to increase the contrast between particles and pores in the platinum film, the vacuum impregnation technique was employed. Unfortunately, this procedure did not result in any significant improvement for feature identification when viewed under the SEM. The result may be due in part to the spatial resolution of the SEM which makes it difficult to develop sufficient contrast between polished platinum particles suspended in a predominantly platinum background.

Examination of the polished paste under an optical microscope, however, revealed that some platinum particles were indeed being polished to such a degree that they reflected light very efficiently. If it is assumed that the reflecting particles (white phase) are representative of the platinum particles in the paste on one plane, then it is possible to conduct a standard image analysis investigation of the cross-sectional area to evaluate the porosity, pore and particle size, as well as the three-phase line.

Table 2 gives the standard morphological parameters for the platinum paste film measured by lineal line scan, and diameter analysis techniques. From these results, it appears that the platinum paste/film has an average particle size approximately 2.3 μm, which is consistent with the manufacturers claim of an average fineness 2-4 μm. This analysis also suggests that the

average porosity is approximately 70% with a three-phase line estimate of approximately 5500 cm/cm². These values, however, are somewhat limited by the optical resolution of the microscope employed (approximately 0.34 μm at 500X) and should be considered relative to the magnification used.

Table 3 compares the properties of several platinum electrodes, as measured by image analysis. The two Engelhard pastes, A-4338 and 6082, exhibit similar particle diameters and three-phase line lengths even though their thermal treatments were quite different. These pastes may also be compared with electrodes formed by sputtering. The thickness of the Engelhard A-4338 film is in the range of 10-40 μm, while those of the sputtered films are 0.75 and 0.3 μm. Again, the thermal and electrical treatments of the paste and sputtered films vary. Nevertheless, the particle diameters are similar and the three-phase line lengths are within an order of magnitude (excluding the sputtered film cured at 973°C).

5.1.2 Profilometry of Platinum Paste Films

Preliminary profilometry work on the platinum films began by examining the surface texture of Engelhard ink #6926. Following examination under SEM it was revealed that the bulk morphology of the films appeared to change with increasing firing temperature. To quantify this effect, small strips, approximately 3 mm x 15 mm were screen-printed on α-alumina substates using the #6926 ink which had been diluted 3:2 with toluene (40%). The test specimens were cured in air at various temperatures ranging from abient (22°C) to 800°C. The surface textures of these films were measured together with their average thicknesses. From the Ra values, it is apparent that there is a significant increase in roughness with increasing temperature. There also appears to be a striking change in film thickness for those pastes cured at > 400°C. These effects agree reasonably well with the SEM observations which show the formation of a metallic coating for temperatures greater than 600°C. As the individual platinum particles sinter together to form interconnected islands, the porosity increases (thereby "roughening" the film) while the thickness decreases. Details of these measurements are available elsewhere [41].

Table 2. - Morphological Parameters for Platinum Paste A-4338 Derived from Image Analysis

	Morphological Descriptor			
Image Analysis Technique	Particle Diameter (μm)	Pore Diameter (μm)	% Porosity	Three-Phase Line (cm/cm^2)
Line Scan (Area)	2.5	-	65 ± 1	5500 ± 250
Lineal	2.2	5.3	72	-
MCD	2.3	3.4	-	-

Table 3. - Comparison of Platinum Electrode Properties

Electrode Material	Composition	Deposition Method	Treatment	Thickness (μm)	Particle Diameter (μm)	Three-Phase Line Length (cm/cm^2)
This study	Engelhard Pt paste A-4338	Brush	100-200°C hydrogen 1 h	10-40	2	5.5×10^3
Ref 29	Engelhard Pt paste 6082	Brush	900°C at 100°C/h	-	1-2	5×10^3
	Pt	Sputtered	1200-1400°C 1 Volt, 1 KHz 5 min.	0.75	-	1.2×10^4
Ref 28	Pt gauze	-	-	200 mesh/cm^2	-	1.4×10^1
	Pt	Sputtered	973°C	0.3	$\leq$ 0.1	$\geq 1.5 \times 10^5$
	Pt	Sputtered	1173°C	0.3	0.5	3×10^4
	Pt	Sputtered	1273°C	0.3	1.0	1.5×10^4

5.1.3 Gas Permeability of Platinum Paste Films

Gas permeability experiments were not conducted on platinum films due to the friability of the uncured pastes and problems associated with preparing the film on a well characterized porous substrate. The difficulty in this approach was the penetration of the platinum ink into the porcus substrate which caused an inaccurate measurement of permeability.

5.1.4 Porosimetry of Platinum Paste Films

Due to the thin nature (~10-20 μm) of the platinum paste films, it was not possible to perform mercury porosimetry on these materials. Attempts could have been made to increase the sample volume by repeated painting of the film, however, the cost associated with such an analysis would have been prohibitive.

5.1.5 Gas Adsorption of Platinum Paste Films

Attempts were made to measusre the surface area of A-4338 platinum paste using the Micromeritics Orr Pore-Volume Surface Area Analyzer by increasing the absolute area present in the adsorption cell. Approximately 200 mm^2 of hand-painted A-4338 paste (on glass slides) was introduced into the customized large adsorption cell for krypton analysis. This corresponds to a total film mass of approximately 0.1 g. Using this appraoch it was not possible to make an accurate reading of surface area. This implies that the surface area of the film must be less than ~3 m^2/g in the uncured state (assuming a sensitivity of 0.01 m^2/g and a total weight (slide and film of 300 g). This would indicate that the unfired platinum film does not appear to have good catalytic properties, most likely due to the presence of organic binders.

5.2 Plasma Sprayed Nickel Films

Preliminary studies of nickel films began by examining the nature of the films produced by the plasma spraying technique. Plasma coatings are known to have a sandwich-like structure and, depending upon spray conditions, can have a variety of pore morphologies. Figures 4 and 5 show a cross-section of a plasma sprayed nickel coating, Ni powder 56C,

supplied by Metco [54] prepared under two different conditions. In Figure 5, the coating was sprayed using an Ar/H_2 plasma (Ar; 6.87 x 10^5 Pascals at 2.52 m^3/h, H2; 3.44 x 10^5 Pascals at 0.283 m^3/h) with a power setting of 60V and 500A. The powder flow was 6 kg/hr and the working distance was 6". The coating shown in Figure 6 was sprayed under identical conditions except that the plasma current was reduced to 300A (thereby decreasing the plasma temperature), and the working distance was increased to 10".

From these figures, it is obvious that there is an apparent increase in total "porosity" caused by decreasing plasma current and increasing working distance. It is interesting to note the nature of the features which are interpreted as "pores" in both of these coatings. Although both films contain a significant number of "large" cavities which actually are pores, the majority of features are long and thin and appear perpendicular to the spray direction.

These structures are probably caused by the formation of metal oxides which are produced on the surface of a molten droplet as it passes through the air. Upon impact, the droplet splatters to form long, thin oxides, commonly referred to as "stringers". Unfortunately, true pores of this shape can also be formed during the film deposition, and distinguishing between these features by conventional examination (SEM or optical) can be extremely difficult if not impossible.

To study the effect of spray conditions (i.e., plasma power and/or working distance) and film thickness on reproducibility, a number of plasma coatings were prepared both in a supported and unsupported manner.

The supported films were prepared at The Technical University of Nova Scotia (TUNS) by spraying Metco powder 56C (nickel) on galvanized steel disks approximately 1" in diameter. The plasma conditions at powder flow were identical to those described earlier (Ar; 6.87 x 10^5 Pascals x 2.52 m^3/h, H^2, 3.44 x 10^5 Pascals x 0.283 m^3/h, 60V, powder flow = 6 kg/hr). The plasma current and working distance were then varied to produce seven coatings for each setting. The settings chosen were; Set 1) 500A, 6", Set 2) 300A, 6", and Set 3) 300A, 10". The thickness of these films as measured by optical microscopy ranges from 0.27 mm to 0.30 mm.

The unsupported films were prepared primarily for permeability measurements in which a free standing film was necessary to remove any substrate effects on gas flow. These films were prepared at The Ontario Research Foundation plasma spray facility by attempting to duplicate the plasma conditions and powder flow employed for the supported films produced at TUNS. The substrates employed, however, were alumina discs approximately 1" in diameter. Previous experimentation at TUNS indicated that if the α-alumina disks were roughened by grit blasting and preheated to remove excess and adsorbed moisture, then nickel could be bonded in a reasonable fashion to the ceramic substrate. If, however, the substrate was not pre-treated (both roughening and heating) then the plasma coatings did not display good bonding characteristics and could be easily removed.

Using this technique, a number of unsupported films of various thicknesses were prepared by increasing the number of passes of spray using a plasma current of 500A and a 6" working distance. Three sets were prepared as follows: Set 1) (1 x double pass), Set 2) (2 x double pass), and Set 3) (3 x double pass). Since each set varies only by the number of double passes, then thicknesses (and hence weights) are expected to increase proportionately. Due to problems of keeping thicker films bonded to the substrate for the period of time to complete all the required passes, the number of suitable samples decreases with the number of passes employed. For this study, six specimens of Set 1), five specimens of Set 2), and two specimens of Set 3), were found acceptable for in-depth analyses. The averaged thicknesses of these unsupported films, as measured by optical microscopy, were: set 1) 0.11 mm, set 2) 0.21 mm, set 3) 0.30 mm.

5.2.1 Image Analysis Plasma Sprayed Nickel Films

In the cross-sectional examination of thin films two planes are commonly employed, thickness and area sections. Figures 5 and 6 are examples of thickness sections which are generally employed to assess both porosity and interfacial bonding. Although some information on pore structure can also be generated from the examination of these sections, it is believed that for porous electrode applications, where the gas flow is parallel to the thickness axis, area

cross-sections may be more indicative of the pores by which the gas molecules must travel. In each case, however, it must be noted that the true pore morphology and degree of tortuosity can only be given by a three dimensional assessment of the complete pore network.

Figure 7 shows a typical optical photomicrograph of a representative field of view for samples analyzed from the three sets of unsupported films prepared at ORF. A qualitative assessment of these cross-sections indicated that they did indeed appear to be similar to the supported film of Set 1 which was produced using identical spray conditions (500A, 6" working distance). Numerical evaluation by image analysis, however, revealed that there was no obvious trend for relating the "porous" structure to film thickness. In fact, the reproducibility of the films, in general, was very low. Table 4 gives the morphological descriptors calculated from an extensive image analysis investigation on these unsupported films. These results indictate that although the thinnest and thickest films (Set 1 and Set 3, respectively) show excellent agreement in all categories, Set 2 appears significantly different in both particle size and porosity.

5.2.2 Profilometry of Plasma Sprayed Nickel Films

It was found that there is little difference between the surface texture of all three film types (within the standard deviations of the average values) which indicates that from a surface texture point of view, increasing the film thickness in a plasma spray operation has no effect on surface roughness.

5.2.3 Gas Permeability

In a previous section, the preparation of unsupported plasma sprayed nickel films was discussed. It was pointed out that in order to conduct permeability measurements on porous films, it is necessary to either support the film on a well-characterized porous substrate whose pore morphology is significantly larger than the test film (to avoid the support becoming the restrictive flow component) or to analyze totally unsupported films.

In this program, permeability measurements were used to evaluate

Table 4. - Morphological Properties via Image Analysis for Unsupported Plasma Sprayed Nickel Films

Sample	IA Technique	Morphological Descriptor			
		Pore Diameter (μm)	Particle Diameter (μm)	Porosity (%)	Three-Phase Line (cm/cm^2)
Set 1	Line Scan (Area)	11.7	-	20.6 ± 4.4	450 ± 70
(1 x double pass)	Lineal	14.9	54.0	21.0	-
	MCD	19.4	60.1	-	-
Set 2	Line Scan (Area)	10.2	-	15.2 ± 3.1	420 ± 70
(2 x double pass)	Lineal	12.6	71.1	14.3	-
	MCD	16.1	66.5	-	-
Set 3	Line Scan (Area)	12.1	-	20.6 ± 5.1	450 ± 90
(3 x double pass)	Lineal	14.9	53.9	20.9	-
	MCD	20.1	60.3	-	-

the reproducibility of preparing porous electrodes using a plasma spray technique as well as to define the effects of changing spray conditions (e.g., plasma power, working distance) on the overall pore morphology. These two conditions are extremely important when one is attempting to produce gas electrodes with identical and controlled morphologies.

To study the similarity of films produced under identical conditions a number of porous nickel coatings were prepared by plasma spraying a non-roughened, non-preheated alumina disc 25 mm in diameter at standard conditions of 500A and 6" spraying distance.

Figure 8 shows the observed flow/pressure curves for six films prepared by a single double pass of the automated spray gun. The films weights varied from 0.25 g - 0.35 g which may have been related to the variability of the gravity feed flow system employed to introduce the nickel powder into the plasma. It is interesting to note, however, that the resistance to flow does not vary, in that a unique pore structure may be generated for each film. This behaviour may be expected since plasma spraying is a truly random process and the build-up of a film is determined by a variety of complex variables (e.g., powder size, flow, plasma temperature, position, etc.). The slopes of the flow curves ranged from 0.123 to 0.182 L/min. psi.

Flow curves were also generated for the six films prepared by two-double passes using the same conditions as for the single pass samples. This corresponded to an approximate doubling of film weight (0.58 to 0.72 g). This increase in film weight and thus the thickness significantly affected the flow characteristics by decreasing the flow rate by almost an order of magnitude. The corresponding slopes varied from 0.011 to 0.025 L/min. psi. Once again, the flow behaviour was very erratic which indicates random and unique pore morphologies. Additional flow curves were produced for the two samples prepared by a three double-pass spray. The variation in flow behaviour was also evident even at these lower flow rates. Table 5 gives the slope of lines determined from the flow curves together with the sample identification and film weight.

These three sets of data as seen in Table 5 indicate that, as

expected, when the weight and thickness of the film is increased there is a significant decrease in gas flow through the material. It does appear, however, that plasma spraying, although capable of producing porous electrode materials, is not a technique by which one can satisfactorily predict the true pore morphology of the resultant film. It is suspected that a more in-depth statistical analysis using many more films could reveal the limits of variability with this process. If this range is found to be satisfactory, then the plasma spray technique could be a viable method of electrode preparation.

5.2.4 Porosimetry

The application of mercury intrusion porosimetry is generally employed for the determination of porosity and pore size distribution in samples with a relatively large void volume. The development of high precision penetrometers during this program has enabled mercury porosimetry analysis to be extended by approximately one order of magnitude into the smaller sample volume end which allows for the partial measurement of pore structure on individual plasma sprayed films. Since it has been shown that the plasma sprayed nickel coatings appear to be rather irreproducible with regard to pore morphology, the ability to measure and compare single films provides another opportunity to investigate the feasibiltiy of the plasma spraying process.

The three types of unsupported plasma sprayed nickel coatings prepared using a different number of spray passes at 500A and 6" W.D. were evaluated. Mercury intrusion porosimetry was conducted from 10 psia to 60,000 psia using the Micromeritics AutoPore 9200 resulting in a pore size range between 18 μm to 0.003 μm.

The cumulative intrusion curves showed the behaviour noted earlier that at high pressures, mercury compression and other effects appear as sample intrusion. To avoid complicating the analysis, the pressure range 30 psi - 1500 psi was chosen, which corresponds to a pore size range of 6 μm - 0.12 μm. This selection omitted the extremely fine pores which were overlapped with compression effects and avoided the larger "pores" (i.e., intrusion between 20-10 μm)

Table 5. - Gas Flow/Pressure Slopes for Unsupported Nickel Plasma Sprayed Films

Sample I.D.		Weight (g)	Slope (Q/P) (L/min.psi)
Set 1	1	0.25	0.182
	2	0.34	0.123
	3	0.32	0.174
	4	0.32	0.165
	5	0.34	0.143
	6	0.35	0.149
Set 2	1	0.66	0.020
	2	0.67	0.016
	3	0.67	0.025
	4	0.69	0.016
	5	0.58	0.022
	6	0.72	0.011
Set 3	1	1.02	0.011
	2	1.08	0.010

which were most likely due to the filling of surface irregularities (e.g., surface texture).

From the intrusion curves, it appeared that there was an increase in the volume of pores approximately 1 μm - 0.6 μm in diameter as the number of passes increased. This effect, however, was complicated by the scaling factors employed. To isolate this effect more clearly, the intrusion volumes (cc/g) for the range 6 μm - 0.12 μm were plotted as Fig. 9. From these curves, there appeared to be a trend that as the thickness of the film is increased there was a shift in pore size (to larger pores) and pore volume.

Each set was repeated (duplicate analysis) and the revised results (30-1500 psia) presented in Table 6. By averaging each of the two porosimetry runs, it was evident that there was, indeed, a trend towards higher porosity with increased film thickness. As the thickness was increased, the average pore diameter also appeared to increase. The pore area, however, remained relatively constant as the surface area for the volume (or number) of larger pores approximated the surface area of the smaller pores.

In an effort to obtain another measurement of porosity of these samples, the degree of mercury entrapment was monitored by recording the increase in weight for the samples following high pressure intrusion. By assuming that the weight change was attributable to mercury being trapped in the pores of the sample, a volume was calculated (based upon the density of mercury) and related to the original sample volume by knowing the theoretical density of nickel (8.90 g/cc) and the sample weight. These measurements are given in Table 6 with the irregular porosimetry results. These results also indicate a trend towards higher porosities with increased film thickness.

At present, this trend is not totally understood, however, one possible explanation may be related to powder segregration in the gravity feed device. As a powder "settles" due to the vibrations in the feeder, smaller particulates will migrate to the bottom leaving larger particle on top. If this takes place in the powder feeder, then with time, the size of particulates entering the plasma will increase in size (assuming a bottomfeed stream), resulting in films

of increased porosity and pore dimension as the spray droplets actually increase in size. This would result in a slight porosity gradient with films that are built up by the multi-pass approach.

5.2.5 Gas Adsorption of Plasma Sprayed Nickel Films

As with the platinum paste films it was necessary to increase the absolute surface area of the plasma sprayed films under study by conducting a multiple-sample analysis using the large adsorption cells. Six sample sets were analyzed corresponding to both the supported (various plasma conditions) and unsupported (thickness variation) films. Krypton adsorption was employed for the analyses and the results are summarized in Table 7.

For the supported films, adsorption on the galvanized steel surfaces was assumed to be negligible due to its non-porous nature, and specific surface area estimates relate to the film weight only. From these results, it appears that there is little significant difference between the films analyzed, with the possible exception of the unsupported three double-pass samples (Set 3). One possible explanation is that with increased working distance the molten droplets have a better opportunity to cool, thereby destroying some microstructural features (e.g., nanopores) which would give rise to an increased surface area. The pore area of approximately 0.07 m^2/g as determined by mercury porosimetry is in good agreement with the surface area of 0.05 - 0.08 m^2/g resulted from gas absorption analysis. In general, however, it appears that the present instrument is still not sensitive enough to distinguish between subtle differences in film surface areas.

5.3 Perovskite Films

As a preliminary investigation, a number of mixed compositon coatings plasma sprayed by the Technical University of Nova Scotia for Electrolyser (Noranda Research Centre) were supplied to ORF [55]. The powders were prepared by a proprietary process which results in a chemical composition of $Co_{0.6}Ni_{0.3}$(316 Stainless Steel)$_{0.1}O_{3-x}$. Figures 10 and 11 [56] shows the surface morphology and cross-sectional nature of these sprayed coatings using plasma

Table 6. - Mercury Porosimetry Analysis of Unsupported Plasma Sprayed Nickel Films (500A, 6" W.D.)

	Set 1 (1 x double pass)		Set 2 (2 x double pass)		Set 3 (3 x double pass)	
Parameter	Sample #4	Sample #6	Sample #6	Sample #5	Sample #1	Sample #2
Intrusion Volume (cc/g) 30 - 1500 psia	0.0065	0.0018	0.0077	0.0088	0.0109	0.0074
Pore Area (m^2/g) 30 - 1500 psia	0.094	0.031	0.089	0.092	0.097	0.081
Average Pore Diameter (30 - 1500 psia	0.28	0.23	0.35	0.38	0.45	0.37
% Porosity (30 - 500 psia)	5.5	1.6	6.4	7.3	8.8	6.2
Average % Porosity	3.6 ± 2.8		6.8 ± 0.6		7.5 ± 1.8	
Mercury Entrapped (cc)	0.0026	0.0029	0.0069	0.0056	0.0105	0.0114
Weight Sample (g)	0.32	0.35	0.71	0.58	1.01	1.07
% Porosity	6.7	6.9	8.0	7.9	8.5	8.7
Average % Porosity	6.8 ± 0.1		7.9 ± 0.1		8.6 ± 0.1	

Table 7. - Specific Surface Areas of Plasma Sprayed Nickel Films

Substrate	Spray Conditions	Specific Surface Area (m^2/g)
Galvanized Steel	500A, 6"	0.075 ± 0.007
Galvanized Steel	300A, 6"	0.064 ± 0.005
Galvanized Steel	300A, 10"	0.067 ± 0.006
Unsupported	500A, 6" 1 x double pass	0.070 ± 0.003
Unsupported	500A, 6" 2 x double pass	0.065 ± 0.001
Unsupported	500A, 6" 3 x double pass	0.048 ± 0.004

conditions of 500A, 55V, 0.305 m working distance, and a 3 kg/hr feed rate.

A portion of this material was sent to the Micromeritics Laboratory where surface area analysis was conducted using the automated Digisorb 2600. This unit operates on the standard multi-point adsorption isotherm (BET) theory for calculating specific surface area, however, as it is entirely micro-computer controlled, the sensitivity of the instrument is increased to measure samples with an absolute area as low as 0.01 m^2. The measured surface area of the $Co_{0.6}Ni_{0.3}(316SS)_{0.1}O_{3-X}$ film was found to be 0.065 m^2/g based upon film weight and assuming that the surface area of the support (Ni mesh) was negligible.

One other composition prepared at TUNS and analyzed by Micromeritics was a plasma coating of $Ni_{0.33}$ $Al_{0.59}$ $Mo_{0.02}O_{3-X}$ which had a surface area of 0.375 m^2/g. This increase in surface area is most likely attributable to the change in the microstructure of the material which was sprayed using plasma conditions of 700A, 70V, 12" working distance and a 2.2 lbs/hr feed rate.

Preliminary plasma tests on the $La_{0.8}Sr_{0.2}CO_{0.8}Ni_{0.2}O_{3-X}$ perovskite powders prepared at TUNS have been able to produce small quantities of the coating supported on nickel mesh. These films had an approximate surface area of 0.3 m^2/g, as measured at ORF using the Micromeritics Orr Pore-Volume Surface Area Analyzer Model 2100.

5.4 Silver Membranes

Difficulties associated with the reproducibility of plasma sprayed films have shown that in order to attempt any correlation between physical characterization techniques, it was essential to employ standardized films with a consistent pore morphology. Silver membrane filters produced by Osmonics [57] were subsequently used to evaluate the various characterization techniques. These metal membranes offered the advantages of relative uniformity, controlled porosity, and pore retention rating (ranging from 5 μm to 0.2 μm), and approximating the physical dimensions of other electrode materials which have been studied in this program (e.g., thicknesses of between 40-70 μm).

Figures 12 and 13 show the virgin surface of a 5 μm filter and demonstrate the morphological nature of these silver membrane filters. The proprietory manufacturing process appeared to be a result of a powder sintering action, possibly in conjunction with a volatile organic pore former. The result was a very porous and tortuous structure with well defined particle retentive abilities.

5.4.1 Image Analysis of Ag Membranes

Five silver membrane pore ratings (5 μm, 1.2 μm, 0.8 μm, 0.45 μm, and 0.2 μm) were selected for in-depth quantitative image analysis using the LeMont OASYS image analysis system. In each case, a 25 mm diameter membrane was prepared by mounting the specimen in standard metallurgical epoxy followed by grinding and polishing it down to the minimum of a 1 μm diamond paste finish. Polished samples were either gold coated for subsequent SEM examination or in some cases (for pore ratings greater than 0.5 μm) analyzed directly by optical microscopy techniques. In both situations, it was necessary to treat or analyze the samples immediately to avoid oxidation (tarnishing) of the exposed silver metal which distorts the pore structure image.

Of striking contrast in the set of cross-sectioned and polished membranes was the difference in the continuous (interconnected) phase between the 5 μm, 1.2 μm, and 0.8 μm membranes as well as between the 0.45 μm and 0.2 μm membranes. In the former case, the voids (pores) appeared interconnected while the solid phase (silver) appeared as isolated particles. The opposite was observed for the finer pore rated membranes in which the pores now appeared as isolated voids and the silver phase is continuous. This had a significant effect on the pore/particles size determination as computed by an area determination. In the case where joined features were of interest, a lineal or chord length analysis was more appropriate for evaluating feature size.

Table 8 gives the mean particle/pore diameter measured by a chord length distribution analysis. In each case, 7 to 10 frames (photomicrographs) were analyzed with 5 lines/frame. This corresponded to between 250 and 500 individual feature measurements.

As can be seen from this table, the particle diameters remain relatively constant while the pore diameters decrease in size. There exists a very good correlation between the pore diameters measured by the lineal approach and the minimum crossing distance (MCD) technique developed specifically for evaluating porous structures. Table 8 also shows the measured average particle diameter using the line scan or area equivalent diameter logic. As with the chord length of line scan analysis, the particle diameters remained relatively constant until the silver particulates became the continuous phase (i.e., pore rating < 0.5 μm) whereupon the measured particle diameters became greatly exaggerated and somewhat meaningless.

The decrease in pore diameter while maintaining a consistent particle diameter results in a decrease in overall porosity. As with the feature dimension analysis, the porosities of the silver membranes can be measured in a number of ways. Table 9 lists the percent porosity for each polished membrane filter using both a line scan (area) technique and a chord length to total length analysis (both voids and particles). From this table, it is apparent that for porous silver membranes with less than approximately 30% porosity, the solid phase becomes continuous.

One other important parameter that can be derived from image analysis is the perimeter-to-area ratio for selected features (either pores or particles). If one were able to examine particles of the electrode situated at the electrolyte (i.e., interface), this perimeter would correspond to the three-phase line. It can be assumed that if a porous body has a random yet uniform structure, such as the silver membranes, then any cross-sectioned plane should approximate any other and hence the three-phase line calculated on any section would be an estimate of the value at the interface. Except for the 5 μm membrane, all the filters have a three-phase line of approximately 6300 cm/cm^2; the 5 μm membrane has a value of 3400 cm/cm^2. This is somewhat expected since, as was shown earlier, the particles remain relatively constant in size while the porosity decreases to account for a smaller pore dimension. Overall, however, the particle perimeter per unit area does not change significantly.

Table 8. - Pore and Particle Diameters for Ag Membranes via Image Analysis

	Pore Diameter		Particle Diameter	
Pore Rating (μm)	Minimum Crossing Distance (μm)	Avg. Chord Length (μm)	Line Scan Area (μm)	Avg. Chord Length (μm)
5.0	3.2	4.3	5.9	4.8
1.2	2.2	2.5	5.8	2.7
0.8	1.5	1.9	4.9	3.4
0.45	1.2	1.2	7.6	3.6
0.2	1.0	1.0	8.5	4.0

Table 9. - Percent Porosity (Voids) for Ag Membranes Determined by Image Analysis

Pore Rating (μm)	Percent Porosity		
	Area Determinations	Chord Length (Particles)	Chord Length (Voids)
5.0	44 ± 9	47	47
1.2	47 ± 4	48	48
0.8	34 ± 2	35	35
0.45	24 ± 6	26	24
0.2	20 ± 2	20	20

5.4.2 Profilometry of Silver Membranes

Initial investigations began by measuring the surface roughness of virgin surfaces for the five silver membranes under study. Samples were mounted on a vacuum holding device developed at ORF as part of this program to secure thin materials. Ten traces were acquired on each membrane using the skidless, standard stylus (approximately 2 μm tip radius) and using the phase corrected mode at a sampling length of 0.08 mm. The small sampling length was chosen to avoid problems in sample leveling which often become dominant when operating in a skidless mode.

It was apparent that there existed a strong correlation between virgin surface texture and particle retention rating for the silver membranes. This effect was most likely attributable to the physical dimensions of the pore diameters. However, it was also complicated by the fact that by using the standard stylus tip, smaller irregularities (e.g., pores) can be under-detected which leads to the interpretation of a smoother surface.

Profilometry was also used to study the thickness and uniformity of the films. In an effort to cross-correlate the porosity measurements observed through image analysis, four silver membrane types were selected for volumetric/gravimetric determination of porosity. Three fresh individual samples of each membrane material were mounted on the vacuum holder such that the filter edge could be easily measured. A minimum of five edges per membrane were measured to provide a reasonably accurate estimate (and standard deviation) for membrane thickness. From this thickness measurement, and by knowing the membrane area (25 mm diameter), a total volume could be computed. This volume was then related to the actual mean weight of a membrane and by using the specific gravity of pure silver (10.5 g/cc), a porosity value could be obtained.

Table 10 lists the measured dimensions and weights as well as the calculated porosity. Only the 1.2 μm weight membrane has a standard error associated with it since three individual membranes were weighed. The other values are an average from the total weight of twenty identical membranes determined during the surface area analysis. The porosity values agree reasonably well with those shown

(see Table 7). The observed deviations are most likely due to the variance in measuring the membrane thickness and weight.

5.4.3 Gas Permeability of Silver Membranes

The five particle retention rated silver membranes were measured for gas flow versus pressure head using helium. Figure 14 shows the excellent fits for the five materials, all of which correspond to the behaviour displayed by other filter membranes, (e.g., Nuclepore and Millipore). Only the 0.2 μm membrane was either sufficiently non-porous or with fine enough pore diameter to produce any significant change in the flow/pressure curve from the blank run.

The 0.2 μm membrane was subsequently selected for investigation of its flow/pressure characteristics using the reactant gases for the "model" fuel cell, hydrogen and oxygen. Figure 15 shows the measured flow curves for the same flowmeter setting. The needle valve into the rotameter tube acted as a flow resistor which limited the gas passage for the various gases. This had the effect of lowering gas flow through the rotameter, depending upon gas composition. The slopes of the flow curves are proportional to the mean free paths of the gas which for oxygen, hydrogen, and helium are 0.099, 0.174 and 0.275 μm, respectively at 20°C and 75 cm Hg [58]. Thus, from equations (3) and (4), the diffusion constant and the current density will be larger for hydrogen than for oxygen if the gas pressure gradient and film porosity are the same.

5.4.4 Porosimetry of Silver Membrane

Because of the formation of a silver-mercury amalgam, it was not possible to conduct a mercury-porosimetry analysis on the silver membranes. Future developments into the area of Wood's metal porosimetry (Bismuth-Lead-Tin-Cadmium compounds) may prove to be useful not only in conducting standard high-pressure intrusion analysis but in the physical characterization of porous bodies by "freezing" the Wood's metal in the pores and then examining the pore shape by SEM/optical image analysis techniques.

Table 10. - Gravimetric/Volumetric Determination of Porosity for Silver Membranes

Absolute Particle Retention (µm)	Weight (g/membrane)	Thickness (µm)	Porosity (%)
1.2	0.126 ± 0.009	52 ± 4	53
0.8	0.170	70 ± 4	53
0.45	0.180	51 ± 5	32
0.2	0.126	37 ± 2	34

5.4.5 Gas Adsorption of Silver Membranes

Due to the small absolute surface area of each idividual membrane and the limit of sensitivity of the Micromeritics Orr Pore-Volume Surface-Area Analyzer Model 2100, it was necessary to increase the sample volume by measuring twenty membranes in unison. Table 11 gives the specific surface areas measured as well as the surface area per unit volume (cm^2/cm^3) of membrane material. The 5 μm membrane was not measured due to the unavailability of twenty virgin samples. Table 11 also lists the estimate of surface area based upon the stereological measurement of the three-phase line (or perimeter) by image analysis. Although the agreement between the B.E.T. technique and image analysis is not as good as one would expect, the values are of the same order of magnitude and agree to within 35%. Possible deviations would be expected due to the inability of the image analysis technique to measure minute crevices or pores which would certainly be accessible by krypton gas adsorption, resulting in an increase in surface area.

6. CONCLUSIONS

The purpose of this study has been to identify, test, and refine characterization techniques for the physical examination of thin film morphology. The five techniques selected in this study for in-depth evaluation have all been shown capable of producing morphological data, providing certain restrictions regarding material types, preparative methods, and the absolute sensitivity of the instruments employed are considered. The interpretation and cross-correlation of this data is somewhat complicated, however, due to film irreproducibility and the destructive nature of some techniques (e.g., mercury porosimetry and impregnation). This has resulted in an assessment of each technique with regard to its practicality (i.e., advantages/disadvantages) in producing reliable information which can be employed to measure the physical properties of porous electrode materials.

6.1 Image Analysis

Image analysis is seen as perhaps the most versatile method currently available for studying film morphology. The technique has

Table 11. - Surface Area of Silver Membrane Filters

Particle Retention Rating (μm)	Specific Surface Area (m^2/g)	Volumetric Surface* Area (cm^2/cm^3)	Stereological** Surface Area Estimate (cm^2/cm^3)
1.2	0.0160	7900	6400
0.8	0.0132	6500	6400
0.45	0.0132	9500	6200
0.2	0.0113	7750	6100

* Based upon thickness values measured by profilometry (See Table 10).
** From image analysis measurement of the three-phase line.

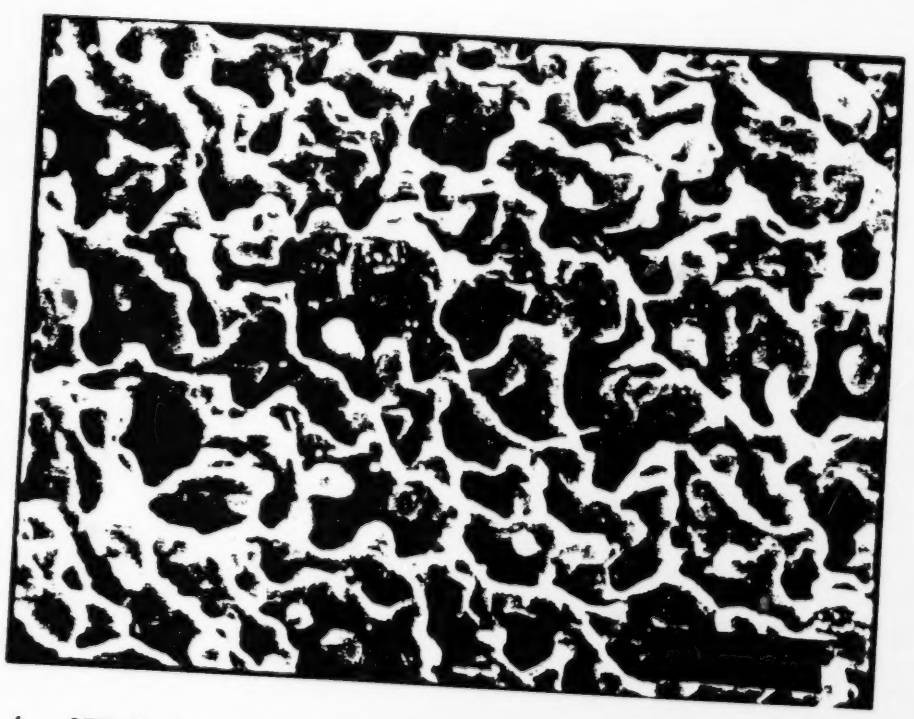

Fig. 4. SEM Photomicrograph of A-4338 Platinum Paste cured at 800°C (approximately 5800X)

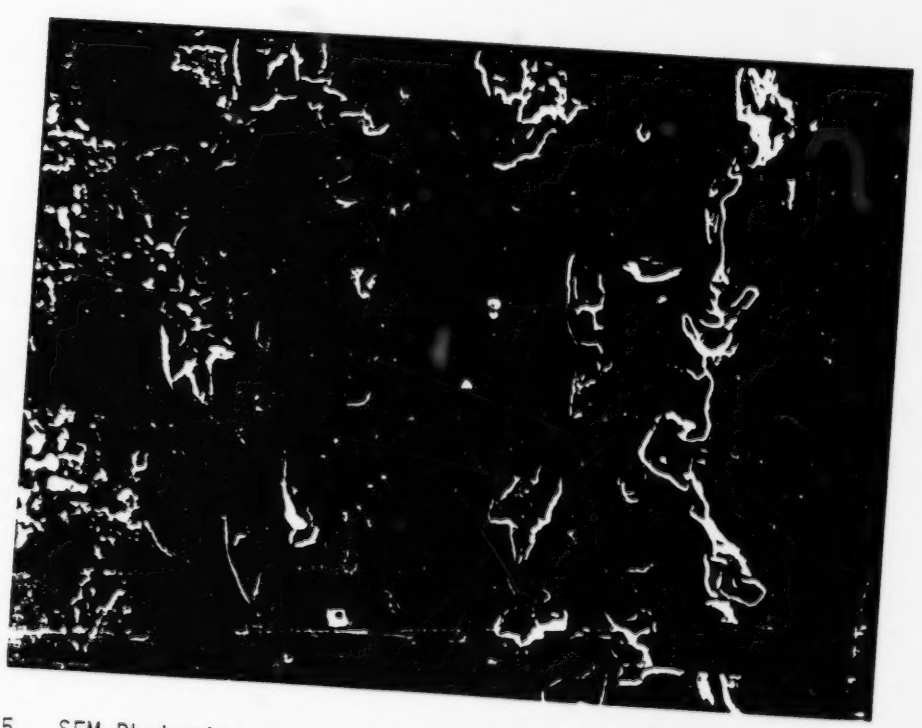

Fig. 5. SEM Photomicrograph of Cross-Sectioned Ni Plasma Sprayed Coating (I = 500 A, WD = 6") Mag approx. 325X

been shown to provide data on all the physical properties which are considered relevant to electrochemical behaviour (i.e., pore size, particle size, pore/particle interface length, and total porosity). The sensitivity of image analysis is limited only by the ability to produce input images of sufficient contrast and resolution. The size of features is generally not considered to be a limitation since atomic-level discrimation can be achieved with state-of-the-art transmission electron microscopy imaging.

The primary limitation of image analysis, as seen in this study, is the difficulty in producing an image which adequately differentiates pores and solids. In materials of simple composition and semi-regular pore structure, such as the silver membranes investigated in this program, standard preparative methods such as epoxy impregnation were found suitable for developing this discrimination. In films with multi-phase components (e.g., oxides in metal plasma films, organics in platinum pastes) or micro-porosity (either low porosity or extremely fine pores), other preparative methods or even alternative image forming techniques (e.g., acoustic microscopy) may be necessary.

Advanced imaging techniques have not been examined in this program, and the imaging methods employed were limited to simple SEM and optical micrographs. These methods were not considered because of equipment/materials availability and the overall objective of the program which was to investigate a number of techniques which would provide relevant physical data on porous films. To this end, the application of image analysis as a technique has been shown to be a viable approach for quantifying important physical features in thin films and should be further examined when relating these properties to electrochemical behaviour.

6.2 Profilometry

Although profilometry makes possible the generation of physical data on thin-film materials in a non-destructive, rapid manner and without the need for involved sample preparation, its application to the direct investigation of bulk film morphology must be viewed in consideration of a number of effects. Profilometry examines surface effects only and is generally applied to the interaction of surfaces with other materials (e.g., bearing ratios, corrosion, erosion). On a

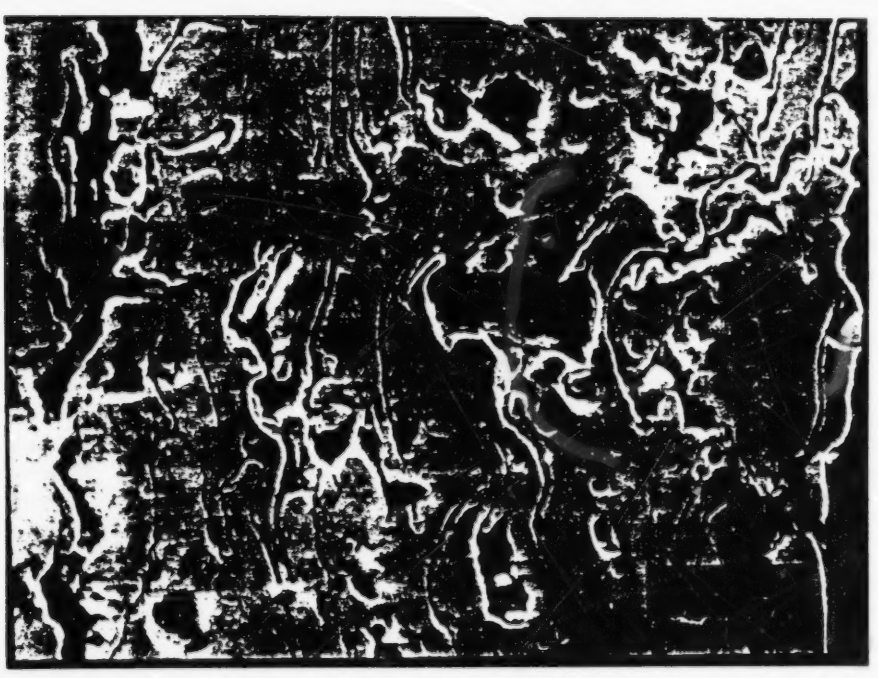

Fig. 6. SEM Photomicrograph of Cross-Sectioned Ni Plasma Sprayed Coating (I = 300 A, WD = 10") Mag approx. 325X

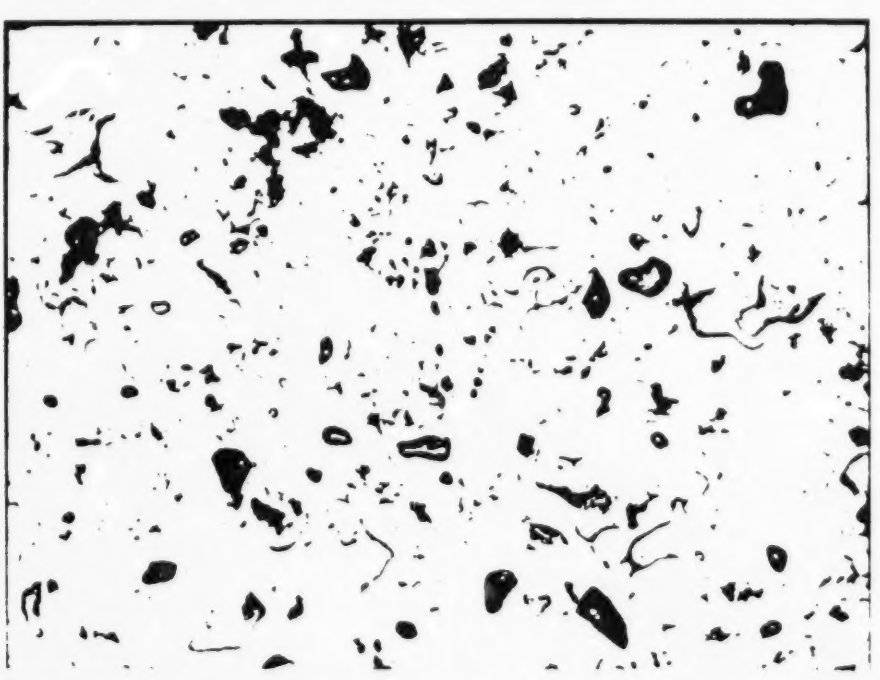

Fig. 7. Optical Photomicrograph of Impregnated/Polished Plasma Sprayed Unsupported Nickel Film (1 x double pass x 500A, 6") Mag = 100X

macroscopic scale, gross deviations in the surface are indeed related to the bulk (e.g., "swiss-cheese") morphology; however, on a microscopic scale, physical forces involved in the formation of a surface may distort the interface such that it does not represent or "mirror" the porous structure contained below. This disparity is particularly evident for films which are formed by methods involving a high degree of surface interaction (e.g., pressing, painting).

6.3 Gas Permeability

Gas permeability offers the simplest means of evaluating a film's total porous nature. Relative differences in the film's physical properties (i.e., thickness, pore size distribution, percent porosity) are easily differentiated with regard to which material and unique morphology can pass a particular volume of a specific gas per unit time. This has obvious consequences when relating the permeability of porous electrodes to the behaviour of electrochemical devices and provides a direct measurement of a film's suitability in this area.

In order to conduct permeability measurements, it is necessary to study unsupported films or films which are supported on a well characterized and highly reproducible substrate. This restricts the application of this technique for the measurement of the flow properties of an electrode directly since most electrolytes (substrates) commonly employed are non-porous and non-permeable. As a result, the films evaluated by peremeametry in this study were of a free-standing nature and no porous substrates were employed. The results have indicated that permeability measurements are particularly useful for studying the variables in producing porous coatings (e.g., plasma films) and for evaluating film reproducibility.

Difficulties encountered in relating theoretical models to the flow behaviour of films indicate that the exact quantificiation of pore dimension is extremely difficult and is controlled by such effects as porosity, tortuosity, pore shape, and thickness. Permeametry has therefore been shown to be best applied in a secondary manner for studying the deposition conditions and reproducibility involved in film production as opposed to measuring actual electrode morphological features.

6.4 Mercury Porosimetry

Traditional mercury intrusion porosimetry using conventional equipment has been shown to have rather limited applications when applied to thin films. The primary limitation of this method is the total sample volume which must be of sufficient quantity to permit detection of the intruded mercury. For the customized penetrometers developed as part of this program, the technique has been shown to be suitable when applied to single films approximately 50 μm or greater in thickness with porosities in excess of approximately 5%. Although the volume of sample can be increased by adding more samples, this has the effect of "averaging" results over large populations which may not be desirable if one is interested in film variability. The technique employed in this study has been shown to be restricted in pore range due to problems resulting from the more sensistive penetrometers. The lower pore size value is presently limited to about 0.1 μm.

Mercury porosimetry was found to be a destructive technique, dependent on pore shape and tortuosity. For the plasma-sprayed nickel films, this method was affected by surface texture. It is also limited by the formation of silver and gold amalgams. The technique does not distinguish between different portions of the sample. This means that thin films are best analyzed when they are unsupported or that the supports must be smooth and non-porous (e.g., glass or metal) in order to avoid affecting the intrusion curves.

Overall, mercury porosimetry cannot be viewed as a practical means of assessing thin-film morphology until alternative methods can be implemented for increasing the sensitivity of measuring the intrusion of mercury into the pores. Although preliminary attempts to make impedence-porosimetry measurements did not result in a usable technique, further study in this area could result in an improved technique for characterizing physical structures.

6.5 Gas Adsorption

As was the case for conventional mercury porosimetry, gas adsorption has been found to be limited by sample size. Through specially designed cells, it has been possible to extend the sensitivity of this technique down to 0.1 m^2. New commercial instrumentation is capable of measuring down to 0.01 m^2. However, in

order to meet the demands of most thin-film applications, where only small amounts of material (e.g., milligrams) are present, a high vacuum system employing ultra-sensitive detection equipment will be necessary.

By increasing the number of samples, and therefore the sample volume, it has been possible to increase the instrumental sensitivity. This practice, however, blends the potential variability of individual films. The limitation of sample size has also negated one of the primary uses of the gas adsorption technique, namely, the determination of pore-size distributions and pore-volume (porosity) measurements through nitrogen adsorption isotherm analysis.

6.6 Correlations of Characterization Techniques

The confidence which can be placed in measurements obtained by a particular technique is determined not only by comparing the theoretical and experimental results for that method, but also by comparing the results with those found from other methods. These comparisons are essential when new materials, processes, and measurement techniques are considered. In this investigation, the five techniques have been employed in various degrees to examine the physical properties of a variety of thin-film materials. In general, the correlation of these techniques has been limited for several reasons. The first and most important cause for the lack of correlation was the non-uniformity of the film materials and their preparation or applications methods. Secondly, when measuring the properties of thin films, there was an obvious limitation of the mass or volume of the film material. In addition to these factors, some of the techniques were destructive so that further measurements of the samples could not be made. Finally, there occurred the difficulty in handling the unsupported films and interference from supported films. An insufficient amount of data was obtained for the platinum paste and perovskite films for correlations to be considered.

With the supported nickel films, permeametry measurements were obviously not performed. The destructive nature of the sample preparation technique for image analysis and of the mercury porosimetry method made comparative testing of the same samples impossible. The presence of contaminant oxides, which appeared as pores, made the image analysis approach a relative technique for the comparison of the plasma

sprayed nickel films. No firm correlation could be established between profilometry and porosimetry for these supported samples.

The unsupported plasma sprayed nickel films show a weak correlation between gas permeability and porosity. Samples within the same set have similar thicknesses and identical preparation conditions. By comparing samples 4 and 6 of Set 1 as well as samples 5 and 6 of Set 2, shown in Tables 4 and 5, it can be seen that an increase in average pore diameter and porosity, as measured by mercury porosimetry, corresponds to an increase in gas permeability. A similar relation was found to exist [41] between the porosity/pore size and surface roughness. In order to be more quantitative, it will be necessary to analyze many more samples.

For the silver membranes which have a well defined porosity, as shown in Table 8, and uniform pore structure, a correlation was found to exist between the pore size, as measured by image analysis, and the surface texture, obtained from profilometry [41]. When Table 8 and Figure 11 are compared, it is seen that a rough correlation exists between the porosity and the slope of the permeability curves for the five membranes. There is also a fair agreement between the porosity data as determined by image analysis and by gravimetric/volumetric measurements as shown in Tables 8 and 9.

Overall, the interdependence of these five techniques appears to be somewhat limited. A better understanding of the importance of these morphological parameters will be obtained by comparing the thin-film properties with electrochemical behaviour. From this comparison, relevant techniques can be selected and refined.

Although the anodic or hydrogen - electrode polarization mechanisms can be neglected for the ZrO_2 and $SrCrO_3$ cells operating in the temperature range of 800-1000°C, these activation and concentration processes will significantly affect hydronium cells operating at 100-300°C. When oxygen is present at the cathode in the fuel-cell mode, its polarization will also be affected by the lower cell temperature. Thus, an understanding of the morphological parameters of both electrodes and their relation to the polarization processes will be essential for effective utilization of hydronium electrolytes. It is evident that the techniques described here will be of value in the determination of these parameters.

REFERENCES

1. Tedmon, C.S., Spacil, H.S. and Mitoff, S.P., J. Electrochem, Soc. 116 (1969) 1170.

2. Yanagida, H., Brook, R.J. and Kroger, F.A., J. Electrochem. Soc. 117 (1970) 593.

3. Etsell, T.H. and Flengas, S.N., J. Electrochem. Soc. 118 (1971) 1890.

4. Brook, R.J., Pelzmann, W.L. and Kroger, F.A., J. Electrochem. Soc. 118 (1971) 185.

5. Pizzini, S., Bianchi, M., Colombo, P. and Torchio, S., J. Appl. Electrochem. 3 (1973) 153.

6. Mari, C., Scolair, V., Fiori, G. and Pizzini, S., J. Appl. Electrochem. 7 (1977) 95.

7. Gur, T., Raistrick, I.D. and Huggins, R.A., J. Electrochem. Soc. 127 (1980) 2620.

8. Mizusaki, J., Amano, K., Yamauchi, S. and Fueki, K., Solid State Ionics 22 (1987) 313.

9. Mizusaki, J., Amano, K., Yamauchi, S. and Fueki, K., Solid State Ionics 22 (1987) 323.

10. Uchida, H., Maeda, N. and Iwahara, H., J. Appl. Electrochem 12 (1982) 645.

11. Iwahara, H., Uchida, H. and Maeda, N., Solid State Ionics 11 (1983) 109.

12. Iwahara, H., Uchida, H. and Tanaka, S., Solid State Ionics 9 and 10 (1983) 1021.

13. Uchida, H., Tanaka, S. and Iwahara, H., J. Appl. Electrochem. 15 (1985) 93.

14. Ahmad, A., Wheat, T.A., Kuriakose, A.K. and Canaday, J.D., Presented at the Electrochemical Society Fall Meeting, New Orleans, Louisiana, October 1984, Division Report ERP/MSL 84-93 (OP&J); CANMET, Energy, Mines and Resources Canada, 1984.

15. Kuriakose, A.K., Wheat, T.A., Ahmad, A. and Canaday, J.D., Presented at the Annual Meeting of the Canadian Ceramic Society, Ottawa, Ontario, February, 1985; Division Report ERP/MSL 85-26 (OP); CANMET, Energy, Mines and Resources Canaday, 1985.

16. Kuriakose, A.K., Wheat, T.A., Ahmad, A. and Canaday, J.D., Division Report MSL 86-58 (J); CANMET, Energy, Mines and Resources Canada, 1986, Submitted for publication in Solid State Ionics (1987).

17. Kuriakose, A.K., Wheat, T.A., Ahmad, A. and Dirocco, J., American Ceram. Soc. 67 (3) (1984) 179.

18. Ahmad, A., Wheat, T.A., Kuriakose, A.K. and Canaday, J.D., Presented at the Annual Meeting of the Canadian Ceramic Society, Ottawa, Ontario, February 1985; Division Report, ERP/MSL 85-22 (OP); CANMET, Energy, Mines and Resources, Canada, 1985.

19. Kuriakose, A.K., Wheat, T.A., Ahmad, A., Canaday, J.D. and Hanson, A.J., Canadian Patent Application 4859464, 1985 June 28.

20. Jenson, J. and Kleitz, M., Solid State Protonic Conductors I, Odense University Press, Odense, Denmark, 1982.

21. Goodenough, J.B., Jensen, J. and Kleitz N., Solid State Protonic Conductors II, Odense University Press, Odense, Denmark, 1983.

22. Goodenough, J.B., Jensen, J. and Kleitz N., Solid State Protonic Conductors III, Odense University Press, Odense, Denmark, 1985.

23. Canaday, J.D., Kuriakose, A.K., Ahmad, A. and Wheat, T.A., J. Canadian Ceramic Soc. 55 (1986) 34.

24. Gulens, J., Longhurst, T.H., Kuriakose, A.K. and Canaday, J.D., Presented at the Sixth International Conference on Solid State Ionics (1987) and submitted for publication in Solid State Ionics (1987).

25. Canaday, J.D., Kuriakose,A.K., Wheat, T.A. and Ahmad, A., Division Report ERP/MSL 86-156 (IR); CANMET, Energy, Mines and Resources Canada, 1986.

26. Munshi, M.Z. and Nicholson, P.S., Solid State Ionics 23 (1987) 203.

27. Wang, D.Y. and Nowick, A.S., J. Electrochem. Soc. 126 (1979) 1155.

28. Verkerk, M.J., Hammink, M.W.J. and Burggraaf, A.J., J. Electrochem. Soc. 130 (1983) 70.

29. Braunshtein, D., Tannhauser, D.S. and Riess, I., J. Electrochem. Soc. 128 (1981) 82.

30. Bockris, J.O.M. and Reddy, A.K.N., Modern Electrochemistry Vol. 2, Plenum press, New York (1970).

31. Wang, D.Y. and Nowick, A.S., J. Electrochem. Soc. 128 (1981) 55.

32. Bard, A.J. and Faulkner, L.R., Electrochemical Methods, John Wiley & Sons, New York (1980).

33. Canaday, J.D., Wheat, T.A., Ahmad, A. and Kuriakose, A.K., J. Appl. Electrochem 17 (1987) 545.

34. Canaday, J.D., Wheat, T.A., Kuriakose, A.K. and Ahmad, A., Int. J. Hydrogen Energy 12 (3) (1987) 151.

35. LeMont Scientific, 2011 Pine Hall Drive, Science Park, State College, PA 16801.

36. Shors, E.C., White, E.W., and Edwards, R.M., "A Method for Quantitative Characterization of Porous Biomaterials using Automated Image Analysis", ASTM Symposium on Porous Implants for Hard Tissue Applications, Nashville, TN, Nov. (1985).

37. MacDonald, W.A., Wheat, T.A. and Quon, H.H., "A Method for the Rapid Mounting and Polishing of Ceramic Materials for Microstructural Examinations", J. Mat Science Letters, 13, p 905 (1978).

38. Spurr Low-Viscosity Embedding Media available from Polysciences, Inc., Warrington, PA 18976-2590.

39. "Rough Surface" ed. Thomas, T.R., Longman Inc, New York (1982).

40. Rank-Taylor Hobson equipment distributed in Canada by Alexander Tools Lts., 215 Carlingview Drive, Unit #304, Rexdale, Ontario M9W 5X8 .

41. Haley, M.P., DSS File No. 03SQ.23440-4-9223; CANMET, Energy Mines and Resources, Canada (1987).

42. Grove, D.M., "Permeability and Flow StudiesJ", Chap. IV in Porous Carbon Solids ed. Bond, R.L., Academic Press, New York (1967).

43. Millipore Limited, 3688 Nashua Drive, Mississauga, Ontario, Canada L4V 1M5.

44. Nuclepore Corporation of Canada, 30 Fordhouse Boulevard, Toronto, Ontario, Canada M8Z 5M3.

45. Dees, P.J., Tjan, T.G., and Polderman, J., "Determination of Pore Diameter by Permeability Measurements", Powder Tech, 27, p 29 (1980).

46. Lowell, S., and Shields, J.E., "Influence of Contact Angle on Hysteresis in Mercury Porosimetry", J. Colloid. Interface Science, 80, p 192 (1981)

47. Svata, M., "Determination of Pore Size and Shape Distribution for Porosimetric Hysteresis Curves", Powder Tech., 5, p 345, (1971).

48. Lowell, S., "Continuous Scan Mercury Porosimetry and the Pore Potential as a Factor in Porosimetry Hysteresis", Powder Tech., 25, p 37 (1980).

49. Micromeretics equipment distributed in Canada by Technical Marketing Associates, 6620 Kitimat Rd., Unit 6, Mississauga, Ontario, L5N 2B8.

50. Cox, B., "A Porosimeter for Determining the Sizes of Flaws in Zirconium or other Insulating Films In-Situ", J. Nuclear Materials, 27, p 1 (1968).

51. Gregg, S.J. and Sing, K.S.W., "Adsorption, Surface Area, and Porosity", Academic, New York (1967).

52. Brunauer, S., Emmett, P.H. and Teller, E., J. Amer. Chem. Soc., 60, p 309 (1938).

53. Engelhard Corporation, Speciality Chemicals Division, 1 West Central Avenue, East Newark, New Jersey 07029.

54. Metco, Inc., 1101 Prospect Avenue, Westbury, Long Island, New York, 11590.

55. Dr. R. LeRoy, Electrolyser Corporation.

56. Compliments of Dr. G. Murphy, Dept of Engineering Physics, Technical University of Nova Scotia, P.O. Box 1000, Halifax, Nova Scotia B3J 2X4.

57. Osmonics, Inc., 5951 Clearwater Drive, Minnetonka, Minnesota 55343.

58. CRC Handbook of Chemistry and Physics, ed. Weast, R.C., ed 56th edition, CRC Press, Cleveland, Ohio (1975).

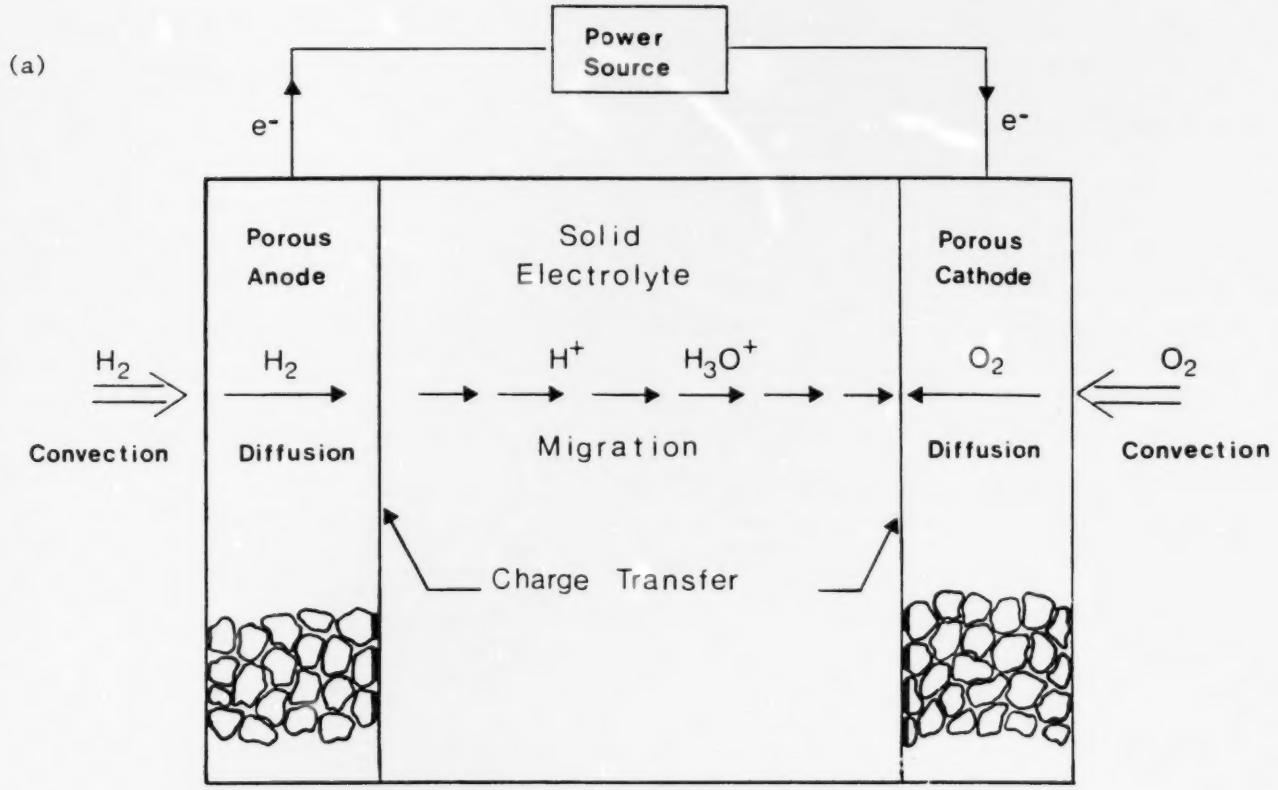

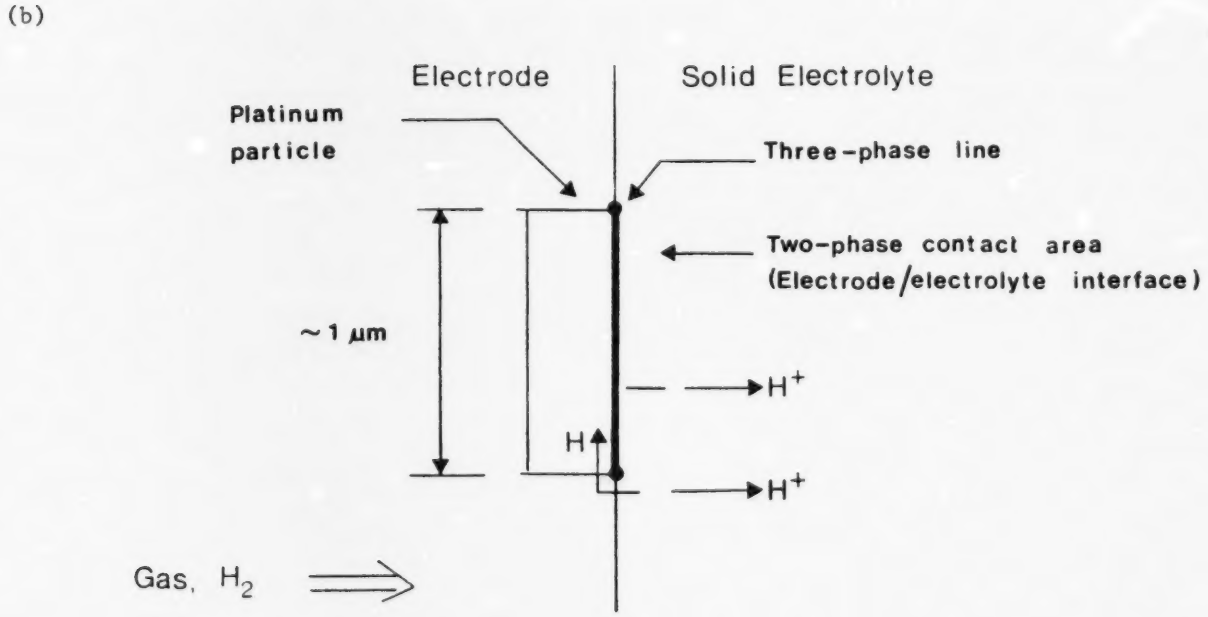

Fig. 1. Schematic diagram of cell (a) with magnified view of interface (b)

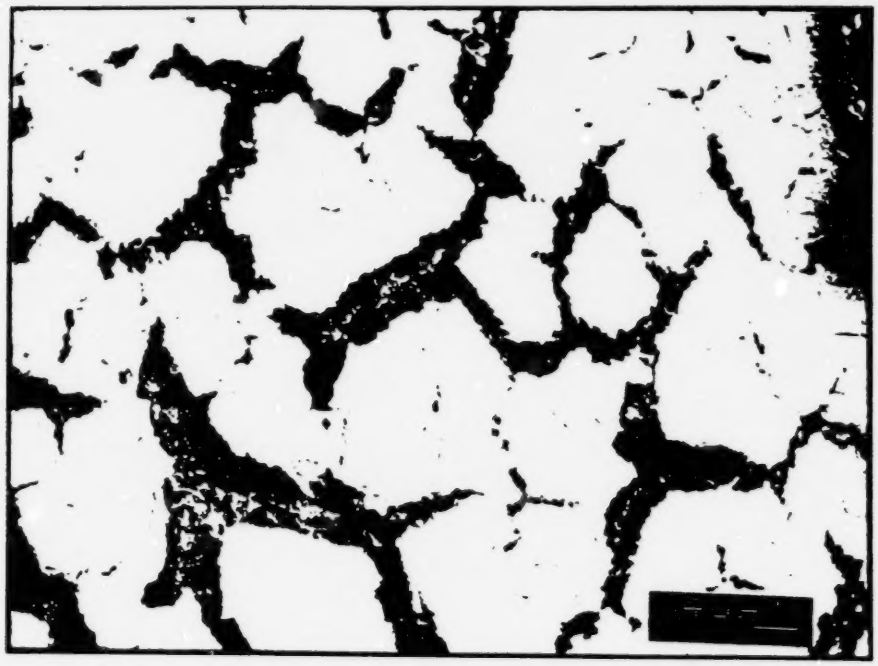

Fig. 2. SEM Photomicrograph of #6926 Platinum Paste cured at 500°C (approximately 150X)

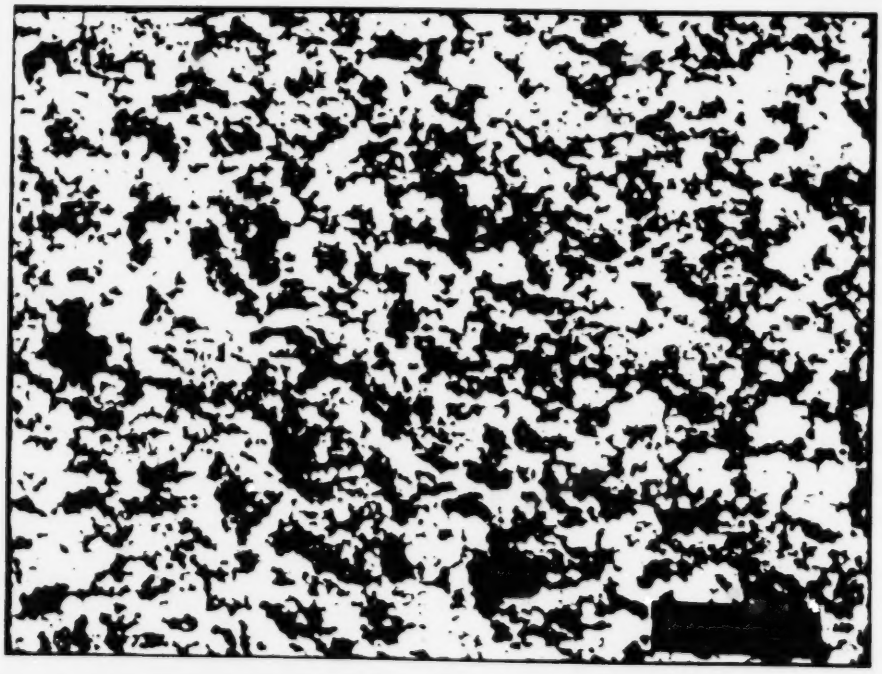

Fig. 3. SEM Photomicrograph of A-4338 Platinum Paste cured at 100°C (approximately 6200X)

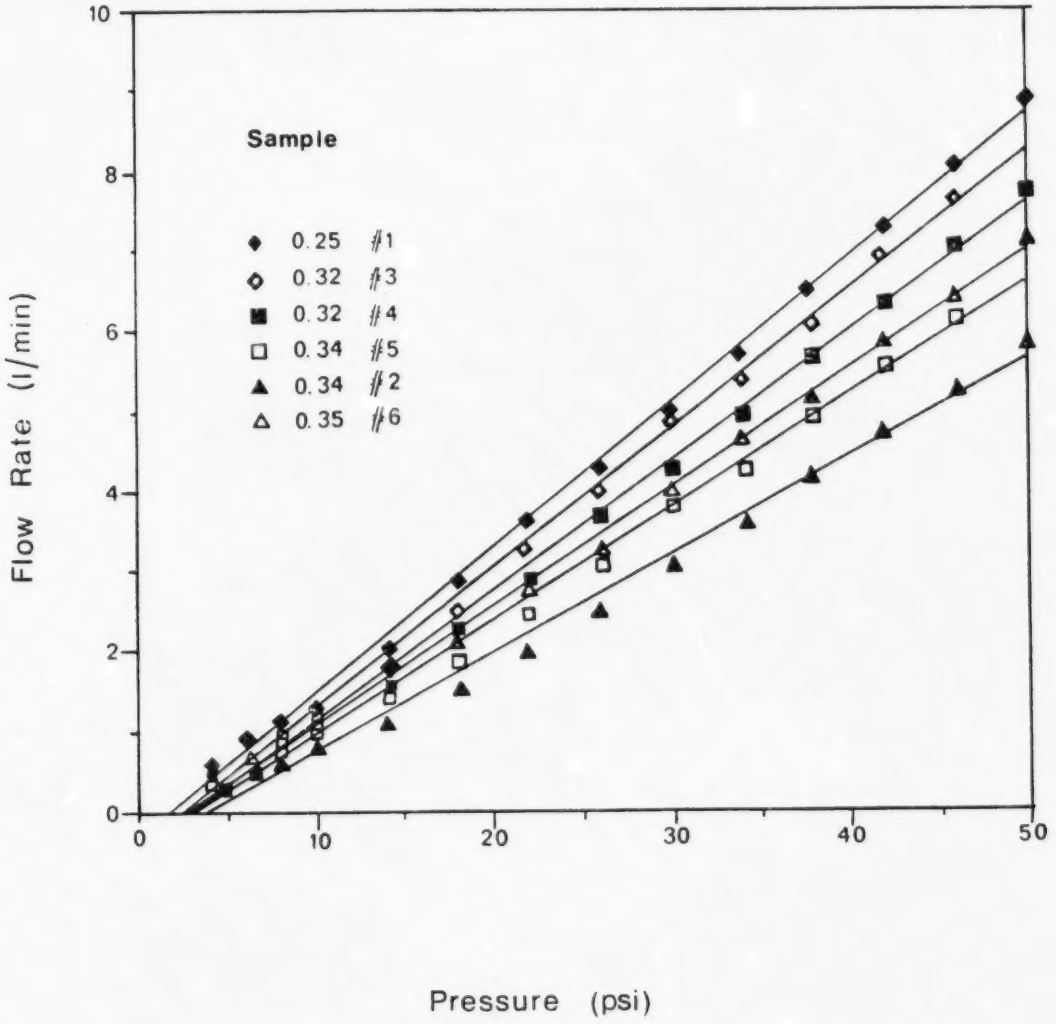

Fig. 8. Permeability Measurements of Set 1 (Single Pass) Unsupported Nickel Plasma Sprayed Films

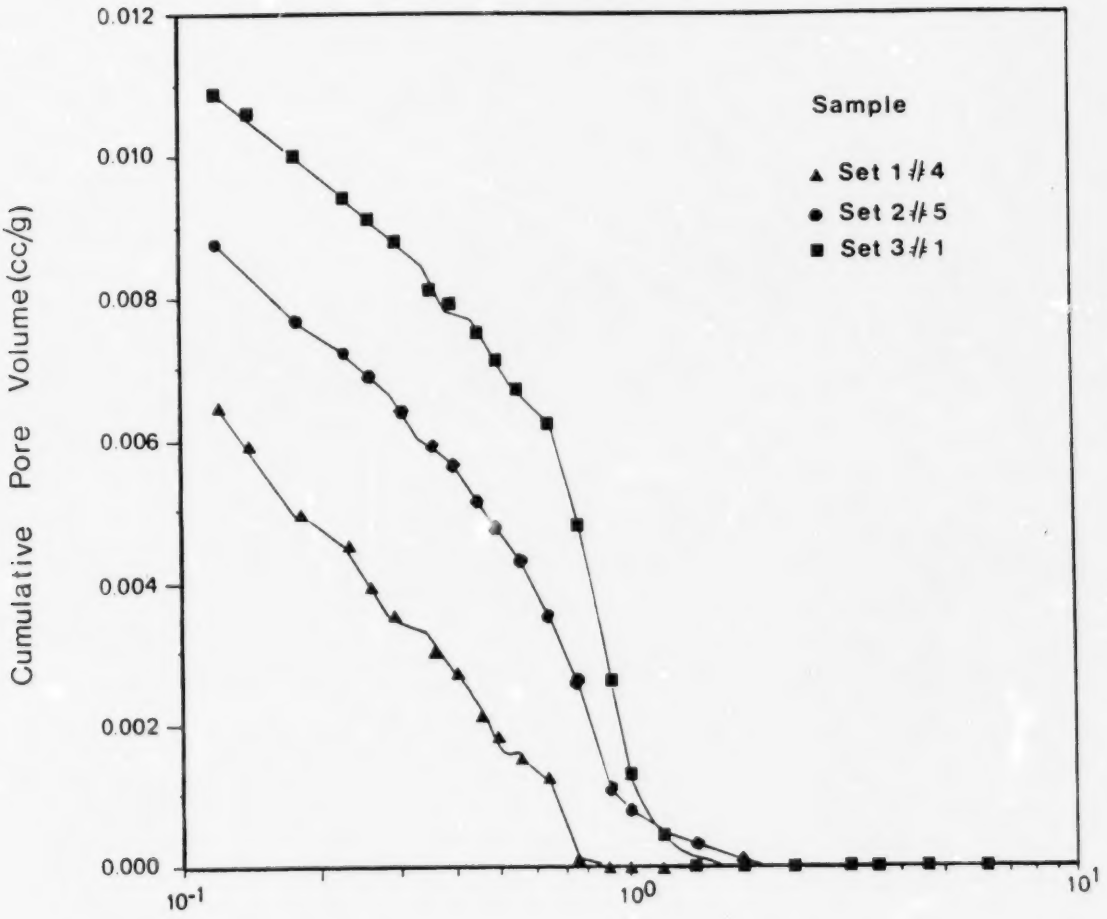

Fig. 9. Mercury Intrusion Curves for Unsupported Nickel Plasma Films

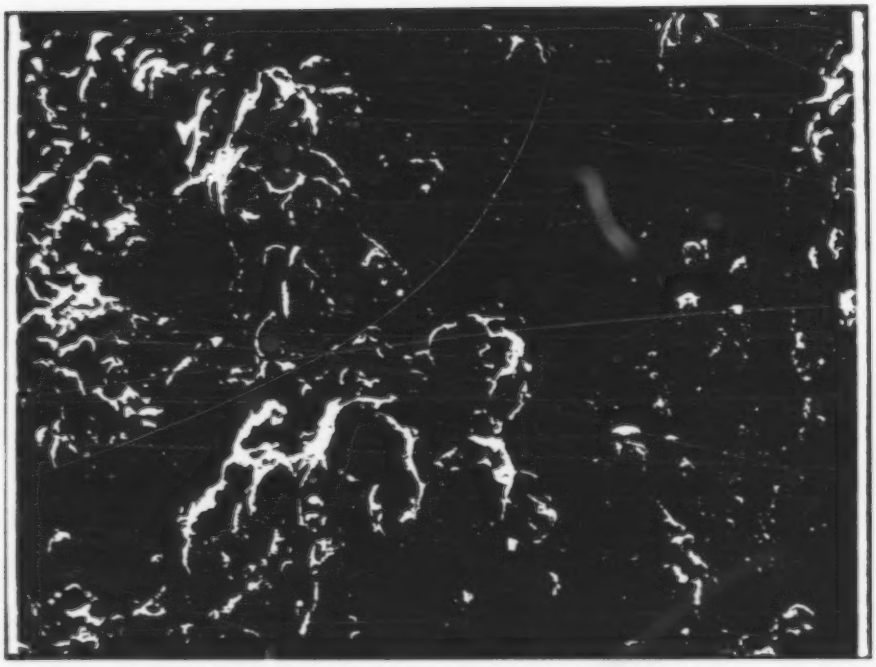

Fig. 10. SEM Micrograph of $Co_{0.6}Ni_{0.3-x}$ Plasma Coating Surface (500X)

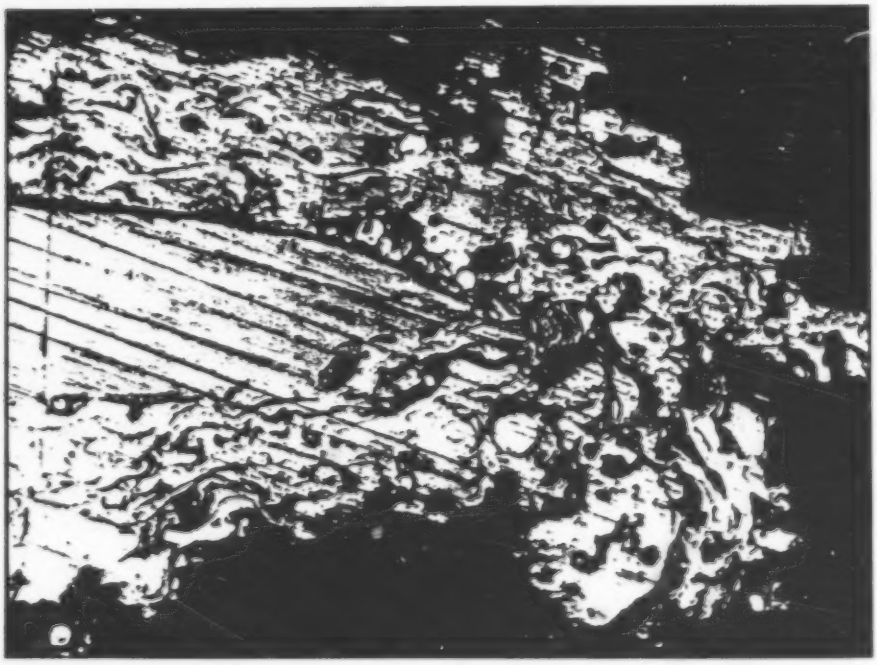

Fig. 11. SEM Micrograph of $Co_{0.6}Ni_{0.3}$ $(316SS)_{0.1}$ O_{3-x} Plasma Coating Cross Section (200X)

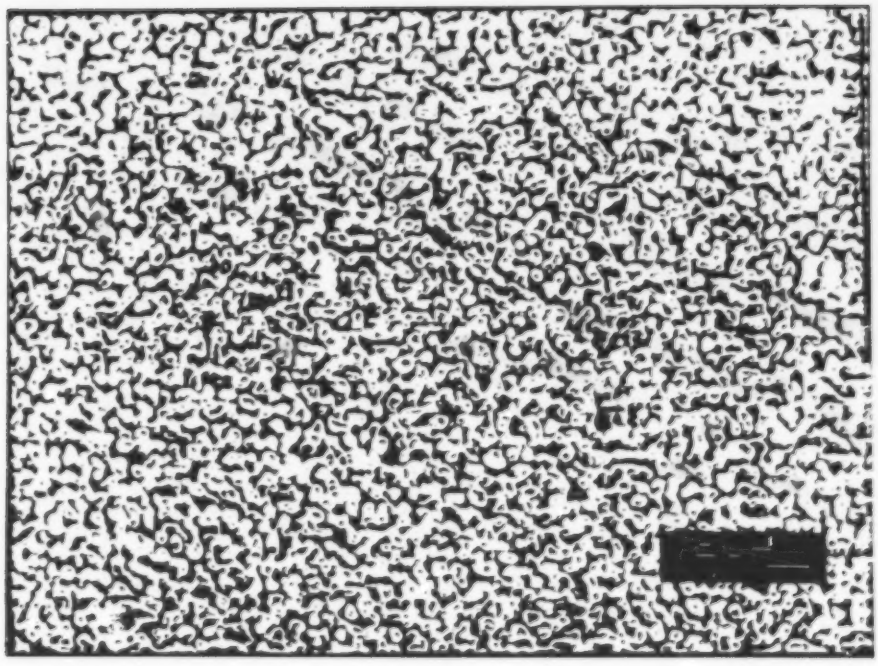

Fig. 12. SEM Photomicrograph of 5 µm Rated Ag Membrane Surface (approx. 300X)

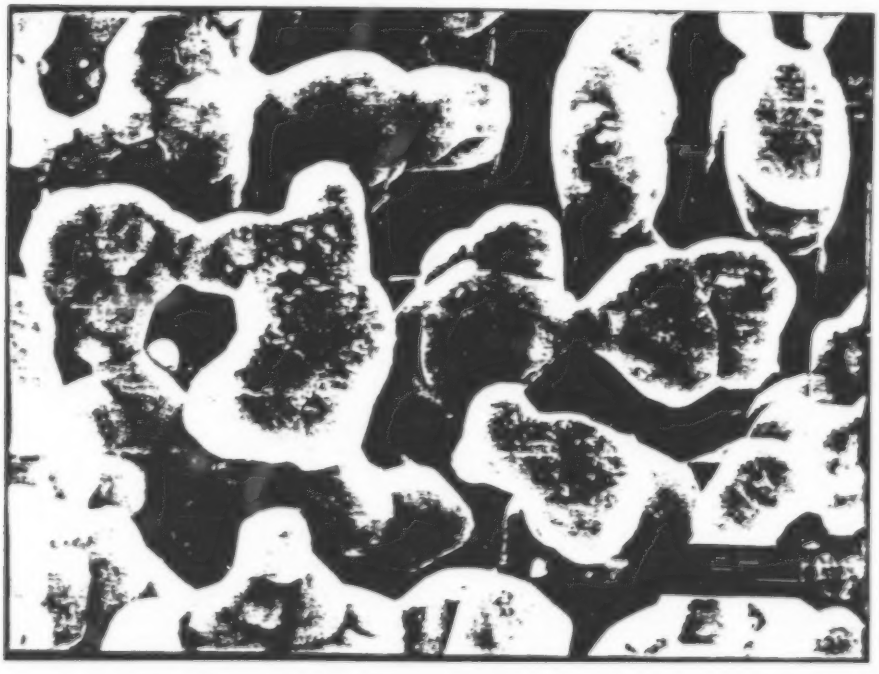

Fig. 13. SEM Photomicrograph of 5 µm Rated Ag Membrane Surface (approx. 3000X)

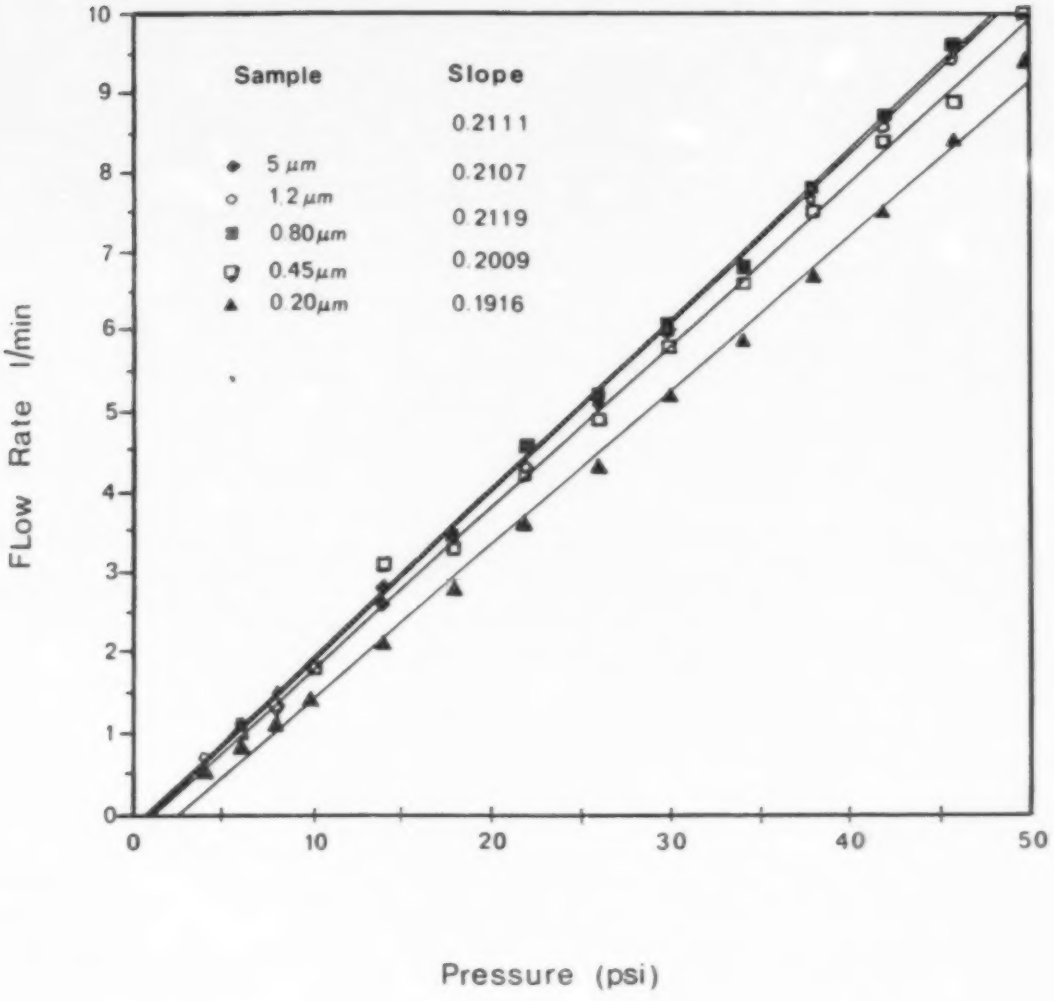

Fig. 14. Permeability Measurements for Silver Membrane Filters (Helium)

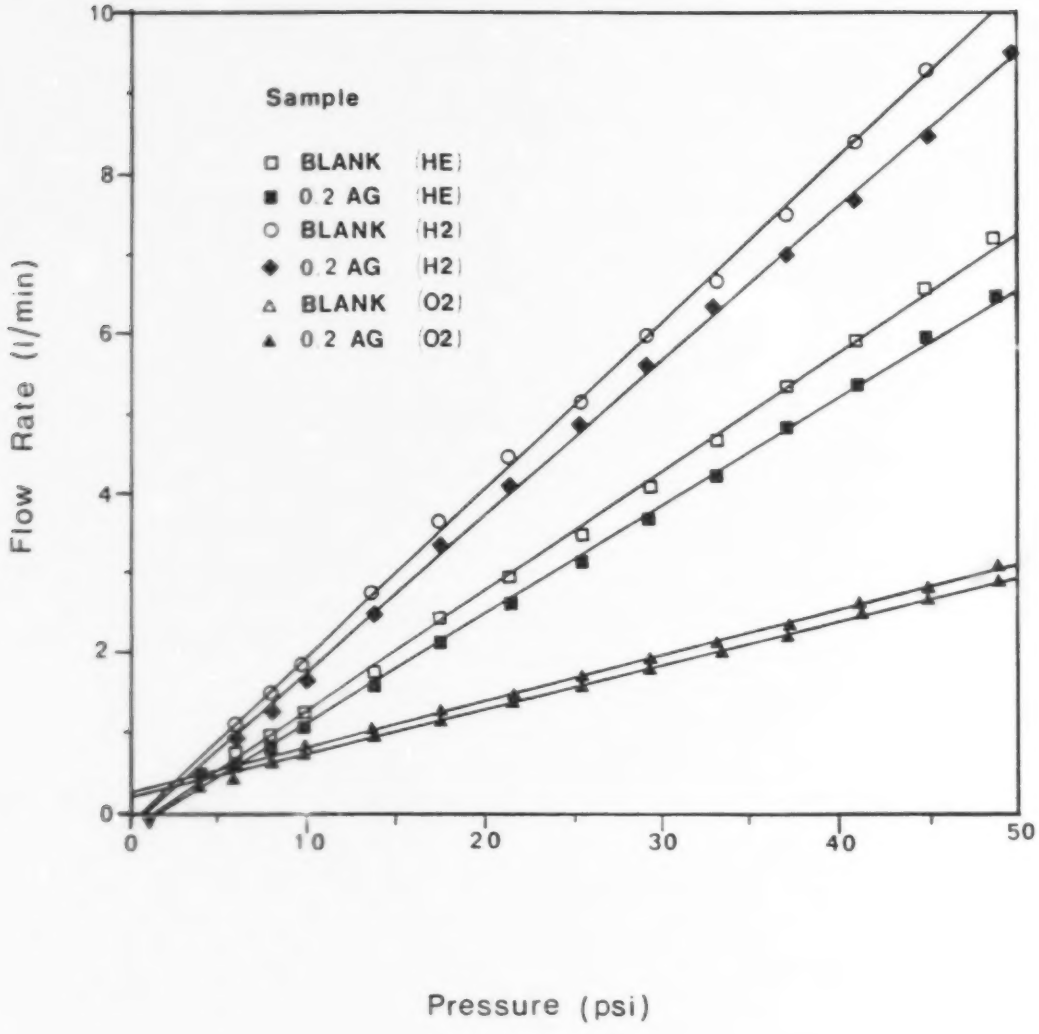

Fig. 15. Comparison of Permeability for 0.2 μm Silver Membrane with Different Gases